About the role of iron on the alteration of simplified nuclear glasses in deaerated solutions at 50°C

Mathieu Brossel, Loïc Marchetti, Patrick Jollivet, Michel Schlegel

About the role of iron on the alteration of simplified nuclear glasses in deaerated solutions at 50 °C

Mathieu Brossel[a,b,c], Loïc Marchetti[a,d,*], Patrick Jollivet[a], Michel L. Schlegel[b]

[a] CEA, DES, ISEC, DE2D, Univ Montpellier, Marcoule, France

[b] Université Paris-Saclay, CEA, Service d'Études Analytiques et de Réactivité des Surfaces, 91191, Gif-sur-Yvette, France

[c] ORTEC, SOM, Aix-en-Provence, France

[d] CEA, DES, ISEC, DMRC, Univ Montpellier, Marcoule, France

* Corresponding author. Full postal address: CEA Marcoule – DES/ISEC/DMRC/SPTC/LDCI, Bât. 166 – BP 17171 – F-30207 Bagnols sur Cèze CEDEX; e-mail address: loic.marchetti@cea.fr

Keywords: glass, iron, leaching kinetics, pH, passivating properties, Fe-silicates

Abstract

The effect of Fe on the alteration of two SiO_2-B_2O_3-Na_2O based glasses (Fe_2O_3-free or containing 3.1 mol.% Fe_2O_3) was studied by measurement of initial alteration rates and long-term leaching experiments at 50 °C in initially pure water or in a 10^{-2} mol.L^{-1} $FeCl_2$ solution. The glass alteration kinetics were monitored by periodical leachate analyses; and morphology, structure and composition of solid alteration products were characterized at the end of long-term experiments (*i.e.* after 323 days).

Iron(III) initially incorporated in the glass strengthens the glass network, leading to a decrease of the initial dissolution rate (from 0.15 to 0.026 g.m^{-2}.d^{-1} at 50 °C). The environment of Fe(III) incorporated into the gel depends on the pH of the leaching solution. A change of Fe(III) coordination from fourfold (*i.e.* charge-compensated by Na^+ ions) to sixfold is expected when the pH decreases. Whatever its coordination, Fe^{3+} hinders the gel restructuring into a passivating barrier. Thus, the addition of Fe in the glass composition ultimately leads to higher alteration extent (≈1.5 times greater after 323 days of leaching in our experiments).

In experiments where Fe cations are provided by the leaching medium (mainly at the +II oxidation state), precipitation of Fe-silicates is systematically observed, as well as an increase in glass alteration compared to experiments led in initially pure water (by a factor slightly less than 2). A drastic change in the average pH of experiments (from ≈9 in initially pure water to ≈6 in $FeCl_2$ solution) is also observed. Among mechanisms proposed in the literature to explain the detrimental effect of Fe-silicates precipitation, it seems that the decrease in pH resulting from this precipitation is the main cause of increase in glass alteration observed in this study.

1. Introduction

In France, after reprocessing of spent nuclear fuel, the residual high level radioactive wastes (HLW) are vitrified. The resulting borosilicate glass (commonly called R7T7 glass) is made of about 40 oxides, including Fe_2O_3 (≈1.3 mol.%), and is stored in stainless steel canisters. These canisters should be disposed in a deep geological repository designed with a multi-barrier setup. In this setup, the glass matrix, the stainless steel canister, the steel overpack and finally the clay host rock define a series of successive barriers against the release of radionuclides into the environment [1]. After corrosion of steel envelopes, the porewater saturating the clay host rock will eventually leach the nuclear glass. Glass leaching is generally described by a succession of different rate regimes related to the nature of the underlying mechanisms [2, 3]. First, interdiffusion leads to ion exchanges between protons from the aqueous medium and alkali from the glass, creating a layer of hydrated glass [4]. The hydrolysis of glass covalent bonds then leads to dissolution of this hydrated glass layer at a high rate, called the initial dissolution rate or forward dissolution rate depending on the experimental conditions under which it is measured. This high rate is maintained as long as the leaching supernatant is sufficiently diluted to prevent any backward effect of dissolved aqueous species on the hydrolysis kinetics [2]. When the Si concentration in the supernatant ([Si]) reaches a sufficiently high value, the dissolution rate of the glass tends to decrease to the so-called residual alteration rate [2]. This rate drop is attributed to (i) the decrease in the hydrolysis reaction affinity with respect to silicic acid H_4SiO_4 [5] and (ii) the formation of a passivating[1] amorphous layer at the hydrated glass surface, commonly referred to as the gel [6]. The passivating properties of this gel depend on its composition and porosity [2, 7], which can be related in particular to the concomitant precipitation of crystallized secondary phases [2]. Indeed, the nature of these secondary phases depends on the elements initially present in the medium or released by glass alteration. Accordingly, the precipitation of crystallized secondary phases can scavenge elements that would otherwise reinforce the gel passivating properties (*e.g.* Si). The precipitation of silicate minerals (phyllosilicates, iron-silicates, zeolites, *etc.*) can thus weaken the gel passivating properties [2, 7], but also affect the reaction affinity [5]; both phenomena sustaining glass alteration [2, 8].

The corrosion of steel envelopes can diversely impact the alteration of nuclear glass [5, 8-10], in particular by promoting the buildup of dissolved Fe cations (mainly at the +II oxidation state) in the groundwater [11-13]. Previous studies suggested that Fe cations dissolved in the supernatant can favor high alteration rates *via* the precipitation of Fe-silicate secondary phases [14-17]. The initial presence within the borosilicate glass structure of Fe, a network former with an oxidation state of +III and located in tetrahedral sites [18-20], also impacts the dissolution rate. Iron seems to decrease the initial dissolution rate (r_0) because of its incorporation in the glass network as $[FeO_{4/2}]^-$ moieties compensated by one Na^+ [21-22]. At higher reaction progress, the role of Fe seems more complex as it appears to be non-linear. The addition of a few percent of Fe_2O_3 to the glass composition significantly improves its leaching resistance [21-22]. However, further increases in Fe_2O_3 doping (by about ten

[1] The term "passivation" is subject to various interpretations in the literature and must be defined before pursuing. In this article, the term "passivation" refers to the formation of an alteration layer on the glass surface, which leads to a decrease in the rate of leaching over time. The passivating properties of a layer therefore refer to its ability to slow down the alteration in a given time.

80 percent or more) lead to deterioration in glass durability and the mechanism behind this effect remains unknown [21-22].

All of these results show that a better understanding of the role of Fe cations on glass alteration kinetics and mechanisms is required, depending on whether Fe is brought by the leaching solution or initially present in the glass. Moreover, the combined effect of Fe present
85 both in the glass and in the supernatant has not been investigated yet. In our study, two simple borosilicate glasses were selected to carry out leaching experiments in solution initially containing or not Fe^{2+}. The first one is a three oxides glass without Fe (SiO_2, B_2O_3, Na_2O) whereas the second one is a Fe^{3+}-containing glass deriving from the previous one. Glass alteration was investigated by leachates chemical analysis and characterization of the
90 solid alteration products.

2. Materials and methods

2.1. Glasses preparation

95 Two borosilicate glasses were prepared for this study. The first one (SBN) is made of SiO_2, B_2O_3 and Na_2O only, whereas the second one (SBNFe) has been obtained by adding Fe_2O_3 to the SBN composition. The Si/B/Na ratios of SBN and SBNFe are close to that of the SON68 glass, an inactive analog of the R7T7 glass [22]. The glasses were obtained by melting adequate mixtures of carbonate and oxide powders in a furnace at 1500 °C for 3 h.
100 Next, a part of the molten glass was poured into a graphite crucible and then annealed for 1 h at 590 °C in order to obtain a glass rod; the remainder was quickly cooled to room temperature. Glass compositions were checked by inductively coupled plasma optical emission spectrometry (ICP-OES) analyses after acidic mineralization (Table 1). The amorphous nature of glasses was verified by X-ray diffraction (XRD).

105 The quickly cooled glasses were crushed and sieved to obtain two powders fractions (for each composition) with particle sizes in the 63-125 µm and the 20-40 µm ranges, respectively. The powders were then cleaned in acetone and absolute ethanol by sedimentation to remove fine particles. The specific surface area (*s*) of the powders was measured by Kr adsorption-desorption according to the Brunauer-Emmett-Teller (BET)
110 method [23] (Table 1).

Monolithic glass coupons were cut from the glass rod to perform surface characterizations after long-term leaching experiments (see subsection 2.2 for details). They were mechanically polished up to 1 µm grain diamond paste, then rinsed in ethanol–acetone binary mixture and finally dried.

115 ### 2.2. Leaching experiments

Deionized water (18.2 MΩ.cm), hereafter referred to as pure water, was used either directly for leaching experiments or to prepare a $FeCl_2$ leaching solution. All leaching experiments were performed at (50 ± 1[2]) °C in polytetrafluoroethylene (PTFE) reactors (Savillex) under deaerated conditions (*i.e.* in Ar or N_2 filled glove boxes) in order to minimize oxidation of Fe^{2+}.

[2] Note that all uncertainties in this article are given for a confidence level of 95%.

The O_2 partial pressure was continuously monitored in the glove boxes and remained stable at about $(6 \pm 2) \times 10^{-6}$ bar.

The initial dissolution regime was investigated by leaching of the 63-125 µm grain size powders exposed to initially pure water without pH control. The slurry was continuously homogenized by a magnetic stirring rod. The initial glass-surface-area-to-solution-volume ratios (S/V) were set at 10 m^{-1} ((0.191 ± 0.002) g of SBN glass for (973.93 ± 0.04) mL of pure water) and 20 m^{-1} ((0.370 ± 0.002) g of SBNFe glass for (988.35 ± 0.04) mL of pure water) for SBN and SBNFe slurries, respectively. Note that setting S/V to a higher value for SBNFe was required to quantify [Si] by colorimetric techniques (see subsection 2.3 for details). It was assumed that the release of all network formers and modifiers is congruent in the experimental conditions investigated here. That is why Si, which is the main cation in the studied glasses, was chosen as the glass alteration tracer for these experiments. The total duration of the experiments was about 9 h. Solution samples were taken approximately every hour. Before each sampling, the pH of the solution was measured at the experiment temperature (50 °C).

Table 1. Compositions (in mol.%) of studied glasses determined by ICP-OES and specific surface areas (s) of the two powders used.

Glasses	SiO_2	B_2O_3	Na_2O	Fe_2O_3	s ($m^2.g^{-1}$)	
					63-125 µm	20-40 µm
SBN	68.8	17.2	14.0	-	$(5.3 \pm 0.5) \times 10^{-2}$	$(16 \pm 2) \times 10^{-2}$
SBNFe	66.6	16.7	13.7	3.1	$(5.4 \pm 0.5) \times 10^{-2}$	$(15 \pm 2) \times 10^{-2}$

The leaching at higher reaction progress was studied by exposing SBN and SBNFe to initially pure water or to a 10^{-2} mol.L^{-1} $FeCl_2$ solution (prepared from $FeCl_2$ salt [Normapur®, Prolabo] dissolved in pure water) at free pH for 323 days. In these long-term experiments, S/V was set at 20 000 m^{-1} and the glass was introduced as a 20-40 µm grain size powder bed. Glass monoliths dedicated to characterization of the alteration layer (see subsection 2.4) were also inserted into the powder bed. The long-term alteration experiments are designated hereafter according to the formalism: (glass name; solution) in which “solution” is replaced by H_2O or $FeCl_2$ depending on whether the experiments are carried out in pure water or in the $FeCl_2$ solution.

Supernatant samples (less than 1 mL) were taken after 1, 3, 7, 14 and 29 days, and then at monthly intervals until the end of the experiments. These samples were systematically filtered (0.45 µm pore size). The pH of the supernatant was measured at 50 °C before each sampling. In the case of experiments in initially pure water, the supernatant samples were fully acidified with 0.5 mol.L^{-1} HNO_3; for experiments in the $FeCl_2$ solution, 50 µL were out-sampled before acidification. The acidified samples were stored in a refrigerator and later analyzed by ICP-OES; the unacidified ones were analyzed directly by ultraviolet-visible (UV-Vis) spectrophotometry in order to determine the Fe aqueous concentration [Fe] (see subsection 2.3 for more details on supernatant analyses). In order to compensate for the loss of leaching solution due to sampling and evaporation, but also the uptake of dissolved Fe in solid phases (in the case of experiments carried out in the $FeCl_2$ solution), “addition

solutions" (*i.e.* pure water or concentrated $FeCl_2$ solution) were added after each sampling[3]. The volume of the leaching solution is thus maintained at a value very close to its initial value throughout the duration of the experiments. The renewal resulting from solution additions is roughly 0.4 vol.% per month.

Experiments were dismantled after a final sampling at 323 days. Glass monoliths and powder samples were rinsed with pure water and dried at room temperature in the glove box. Visual observation of the leachates suggested the presence of precipitates in suspension in the case of experiments carried out in the $FeCl_2$ solution. These precipitates were collected by filtration on a cellulose acetate filter (0.45 µm pore size, Sartorius). This last type of solid sample was not rinsed but dried in a similar way than monoliths and powders. All solid samples (Figure 1) were stored under the glove box atmosphere until characterization.

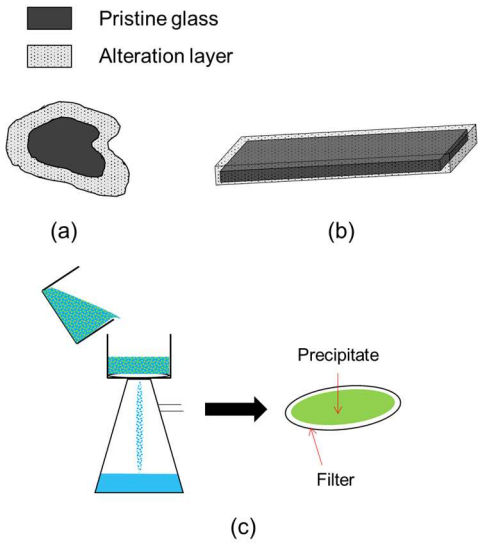

Figure 1. Sketch of different solid samples obtained after 323 days of leaching: a) and b) altered glass powder and monolith, c) precipitates in suspension recovered on a cellulose acetate filter.

2.3. Solution analyses and data processing

For all the experiments, the pH was measured at 50 °C with a Methrom 827 pH lab calibrated using NIST 7 and NIST 9 buffers.

For experiments investigating the initial dissolution regime, [Si] values were determined by UV-Vis spectrophotometry with a Varian Cary® 50 Scan spectrophotometer using the Merck Spectroquant® Silicate Test kit (more details on this colorimetric method are given elsewhere [24]).

For experiments run at a higher reaction progress, two types of analyses were carried out.

To compensate Fe uptake in the case of experiments in the $FeCl_2$ solution, [Fe] were determined directly after sampling by UV-Vis spectrophotometry using the Merck

[3] Note, however, that systematic analyses of [Fe] by UV-Vis spectrophotometry were implemented from the 5th sampling of $FeCl_2$ solutions only. Before these analyses were implemented, it was assumed that all dissolved Fe was consumed between two samplings. The amount of $FeCl_2$ added before the 5th sampling was therefore intended to balance this assumed consumption.

Spectroquant® Iron Test kit. All Fe ions were reduced to the +II oxidation state by ascorbic acid and reacted with 1,10-phenanthroline to form a complex with an absorbance measured at 500 nm. Note that several analyses were duplicated: one performed as described previously and one performed without adding ascorbic acid. This was intended to distinguish Fe^{2+} cations from Fe^{3+} cations in solution. All the double analyses showed that Fe cations present in solution were almost exclusively in the +II oxidation state[4]. Nevertheless, the presence of Fe^{3+} in the system cannot be excluded considering the O_2 partial pressure prevailing in the glove boxes (*cf.* subsection 2.2). Indeed, the Fe cations initially in the +III oxidation state (*e.g.* those coming from the glass) will not change their oxidation state under this O_2 partial pressure.

In order to characterize the glass alteration kinetics in all long-term experiments, the aqueous concentrations of Si, B, Na and Fe were analyzed by ICP-OES using an iCAP™ 6300 Duo spectrometer (Thermo Scientific™).

The aqueous concentration data on elements released during the alteration of glasses was then processed according to the method described below.

The amount of the element *i* released in the supernatant (n_i^{rel} in mol) at the sampling time *t* (corresponding to the k^{th} solution sample taken) was first calculated iteratively from the measured aqueous concentration of *i*, without omitting all mass losses due to sampling:

$$n_i^{rel}(t) = [i]_k \, V_{bs,t} + \sum_{l=1}^{k-1} [i]_l \, V_l \qquad (1),$$

where, $[i]_k$ and $[i]_l$ are respectively the aqueous concentrations of *i* in the k^{th} solution sample and in all previous solution samples; $V_{bs,t}$ is the volume of leaching solution before sampling at time *t* and V_l is the volume of the l^{th} solution samples.

The altered glass fraction f_{AG}^{j} (where *j* specifically refers to the element chosen as the glass alteration tracer) at the sampling time *t* was then calculated according to Eq. (2):

$$f_{AG}^{j}(t) = \frac{n_j^{rel}(t) \, M_j}{m \, x_j} \qquad (2),$$

where M_j is the molar mass of *j*, *m* is the mass of glass used for the experiment and x_j is the weight fraction of *j* in the glass composition. As previously stated, the alteration tracer chosen for studying the initial dissolution regime is Si; whereas B was preferred for long-term experiments because it is not [25] or scarcely retained in the alteration layers (see subsection 3.2.1 for details).

The normalized mass loss of element *i* released in the supernatant by glass alteration (NL^i) at the sampling time *t* is derived from $n_i^{rel}(t)$ according to Eq. (3):

[4] Note that whenever we mention Fe cations present in the supernatant thereafter, it implies that these cations are mainly in the +II oxidation state even when this is not explicitly specified.

$$NL^{i}(t) = \frac{n_i^{rel}(t)\, M_i}{S_G\, x_i} = \frac{n_i^{rel}(t)\, M_i}{s\, m\, x_i} \qquad (3),$$

where S_G (m^2) refers to the initial glass surface area. In the case of initial dissolution regime investigations, r_0 ($g.m^{-2}.d^{-1}$) values were derived from the linear regression of NL^{Si} ($g.m^{-2}$) versus t (days).

For long-term leaching experiments, the equivalent altered glass thickness L_{AG}^{eq} at the end of the reaction period t_f was estimated by approximating the glass powder as a set of spheres of identical radii with a specific surface area equal to that measured for the real powder [26]:

$$L_{AG}^{eq} = \frac{3}{\rho\, s}\left(1 - \left(1 - f_{AG}^{B}(t_f)\right)^{1/3}\right) \qquad (4),$$

in which ρ stands for the density of the glass, *i.e.* (2.5 ± 0.1) $g.cm^{-3}$ and (2.7 ± 0.3) $g.cm^{-3}$ for SBN and SBNFe respectively.

Finally, for experiments in the $FeCl_2$ solution, the amount of dissolved Fe consumed during glass alteration (n_{Fe}^{c} in mol) at the sampling time t (k^{th} solution sample) can be calculated as:

$$n_{Fe}^{c}(t) = [Fe]_0\, V_0 + \sum_{l=1}^{k-1} [Fe]_l^{ad}\, V_l^{ad} - \left([Fe]_k\, V_{bs,t} + \sum_{l=1}^{k-1} [Fe]_l\, V_l \right) \qquad (5),$$

in which V_0 and $[Fe]_0$ are the initial volume and Fe concentration of the leaching solution, respectively; and V_l^{ad} and $[Fe]_l^{ad}$ are the volume and the Fe concentration of the $FeCl_2$ aliquot added to the slurry after the l^{th} solution sampling for Fe consumption compensation purpose (see subsection 2.2 for details).

2.4. Solid characterizations

The morphology of the alteration layers was characterized by scanning electron microscopy (SEM) using a Zeiss Merlin microscope equipped with a field emission gun (FEG) and operated at an acceleration voltage of 15 kV. This microscope is equipped with an energy dispersive spectrometer (EDX) for local elemental analyses (EDAX, EDEN Instruments). SEM investigations were carried out on two types of cross-sections (Figure 2). The first one corresponds to a monolith on which the surface of the alteration layer was first marked by sputtering a thin coat of Au. The monolith was then wrapped in an aluminum foil before being embedded in a resin (the Al foil prevents the separation between the alteration layer and the pristine glass by the shrinkage of the resin). The embedded monolith was sectioned and the cross-section was ground using silicon carbide papers, then polished with 9 µm and finally with 1 µm diamond suspensions (Figure 2a). Gold was ultimately sputtered on polished cross-sections to ensure a good conductivity of the sample. SEM observations were also performed on fractured cross-sections without surface preparation except gold sputtering for conduction purpose. For these last observations, the sample is put on a tilted sample holder (Figure 2b).

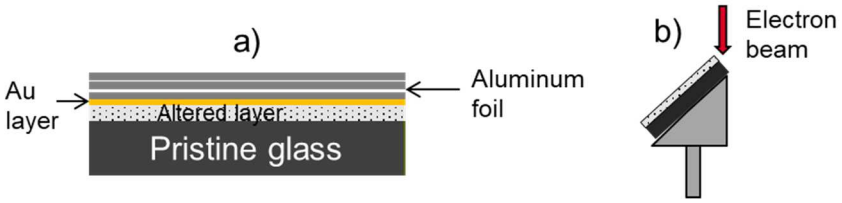

Figure 2. Sketch of the two kinds of samples characterized by SEM: a) polished cross-section and b) fractured cross-section put on a tilted sample holder.

The crystallographic structure of the secondary phases possibly formed during glass alteration was investigated by XRD using a Philips Xpert diffractometer equipped with a molybdenum anode ($K_{\alpha 1}$ = 0.70932 Å) operating at 60 kV and 40 mA. XRD patterns were recorded for 2θ values ranging from 4° to 80° with a 0.017° step size at a scanning speed of 0.11 °.min^{-1}. Altered glass powders from (SBNFe; H_2O), (SBN; $FeCl_2$) and (SBNFe; $FeCl_2$) experiments were measured in Bragg-Bentano configuration (θ/2θ mode). The precipitates collected on a cellulose acetate filter for the (SBN; $FeCl_2$) experiment were measured in fixed incidence mode (incidence angle of 2°) using a sample holder made of silicon.

Glow discharge optical emission spectrometry (GD-OES) and time-of-flight secondary ion mass spectrometry (ToF-SIMS) were employed to determine Si, B, Na and Fe depth elemental profiles in the alteration layers. These analyses were led on monolithic samples. Regardless of the characterization method, the average crater depth was measured after each analysis with a mechanical profilometer. Relating the crater depth to the analysis time allowed the conversion of signal *vs.* time profiles into signal *vs.* depth profiles assuming that the sputtering rate remained constant over time. This hypothesis seems reasonable because the silicate network does not evolves dramatically between the gel and the underlying pristine borosilicate glass during alteration under experimental conditions close to those implemented in this study [7, 27-28].

To the authors' knowledge, GD-OES has never been used before to perform elemental profiling through alteration layers formed on the surface of leached glasses. GD-OES is based on the formation of an Ar plasma between an anode and the sample surface, acting as a cathode. The sample surface is sputtered by Ar^+ ions, then sputtered atoms enter the plasma where they are excited and emit photons. Thus, the advantage of GD-OES in the present case is that the emission yields of the sputtered atoms are independent of the matrix [29]. Consequently, the raw data obtained by this characterization method are generally easier to quantify than those obtained by ToF-SIMS, since the ionization yield may, conversely, strongly depend on the matrix [30-31].

GD-OES analyses were performed on glass monoliths from (SBN; H_2O) and (SBNFe; $FeCl_2$) experiments using a Horiba Jobin Yvon GD-Profiler 2. The discharge source was used under an Ar partial pressure of about 800 Pa. The Cu anode diameter is 4 mm and the input power, delivered by a radiofrequency (RF) generator, was adjusted to 40 W. In addition, in order to facilitate plasma priming on the surface of the altered glass samples, a magnet was placed between the sample back face and the RF source. In order to derive quantitative depth elemental profiles from raw data collected by GD-OES, the method of quantification proposed by Pons-Corbeau *et al.* [32] has been applied using coupons of pristine SBN and SBNFe as standards.

ToF-SIMS analyses were carried out on glass monoliths from (SBNFe; H_2O), (SBN; $FeCl_2$) and (SBNFe; $FeCl_2$) experiments using a TOF.SIMS 5 (IONTOF GmbH®). During the abrasion sequences, a 1 keV primary O_2^+ ion beam (270 nA) sputters a crater over 200×200 µm² whereas the analyzed surface was limited to a 50×50 µm² area located at the center of the crater. The analysis sequences were performed using a 25 keV Bi^+ ion beam at 1.5 pA. During analyses, charging at the sample surface was compensated by low-energy electrons (< 20 eV) delivered by a flood gun. The method proposed by Pons-Corbeau *et al.* [32] (using pristine SBN and SBNFe coupons as standards) to quantify GD-OES profiles has also been applied in order to obtain quantitative data from ToF-SIMS raw profiles. This assumes that the ionization yields associated with the analyzed secondary ions are similar whether they are emitted from the alteration layer or from the pristine glass. In the present case, this hypothesis seems reasonable as a first approximation because, as discussed above, the silicate networks of the pristine glass and the gel formed in this study should be similar enough [7, 27-28]. Nevertheless, in order to check the validity of this assumption, GD-OES and ToF-SIMS quantified profiles obtained on two monoliths from the same experiment (*i.e.* the (SBNFe; $FeCl_2$) experiment) were compared in Section 3 (see subsection 3.2.1.1 for details).

The O profile was also recorded by GD-OES, but not by ToF-SIMS, due to the use of the O_2^+ ion beam during the abrasion sequences. The O data were therefore excluded from the normalization of GD-OES data, in order to permit direct comparison of the Si, B, Na and Fe quantified profiles derived from GD-OES and ToF-SIMS analyses. It is however evident that O remains the main element in all the compounds studied in this work (glass, gel, secondary phases...).

3. Results and discussion

3.1. Effect of the glass composition on the initial dissolution rate

The evolutions of [Si] and NL^{Si} as a function of time resulting from leaching experiments led on SBN and SBNFe in the initial dissolution regime are shown in Figure 3. Note that the two experiments were conducted for different S/V (10 m^{-1} and 20 m^{-1} respectively for SBN and SBNFe glasses). However, the [Si] values remain rather close in both experiments (≈0.005 mmol.L^{-1} and ≈0.002 mmol.L^{-1} at the end of experiments led on SBN and SBNFe respectively) and in any case very far from the solubility of amorphous silica at the temperature and pH of the experiments (*i.e.* ≈3 mmol.L^{-1} [16]). A similar pH increase during both experiments, from 6.8 ± 0.1 to 7.3 ± 0.1, was also observed. However, this variation seems small enough to have only a weak impact on the evolutions of NL^{Si} *vs. t* curves. Indeed, the curves reported in Figure 3 exhibit linear trends, although the slope of these curves (*i.e.* r_0) is in theory pH-dependent [2, 33].

Although the experiments carried out on SBN and SBNFe were conducted for different S/V, they resulted in similar variations in pH and [Si]. It was therefore assumed that the values of r_0 deduced from these experiments could be compared. The evolutions of NL^{Si} *vs. t* show that the initial dissolution rate is higher for SBN than for SBNFe, which is confirmed by r_0 values (Table 2). The same trend is observed during the first days of long-term leaching experiments, as shown in subsection 3.2.2. These results show that Fe incorporated in the glass slows its alteration during the initial dissolution regime. This is in agreement with previous work revealing a similar effect of Fe incorporated in simple glasses close to those

investigated here (SiO_2-B_2O_3-Na_2O based glasses with different Fe_2O_3 contents) [22]. Such an effect was also observed for the more complex MW borosilicate glasses developed in the United Kingdom to immobilize high-level radioactive waste [21].

This result could be explained by the presence in the glass structure of $[FeO_{4/2}]^-$ tetrahedral moieties, the charge of which is balanced locally by Na^+ [20, 22]. Because Na^+ ions balancing $[FeO_{4/2}]^-$ units can no longer compensate non-bridging oxygen (NBO) of silicate tetrahedra, the number of NBO per SiO_2 tetrahedron decreases with increasing Fe content. This implies a better durability of the Fe-containing glass matrix against hydrolysis reactions involved in the initial dissolution regime, as previously proposed in the litterature [22].

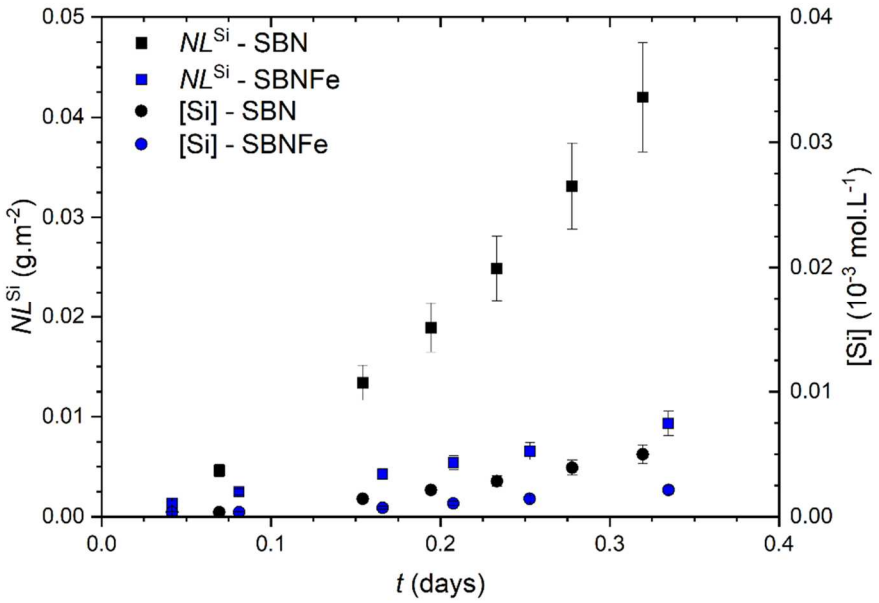

Figure 3. Evolutions of NL^{Si} and [Si] *vs.* time in the case of SBN (S/V =10 m^{-1}) and SBNFe (S/V =20 m^{-1}) altered in initially pure water at 50°C and free pH.

Table 2. Values of r_0 at pH ≈7 derived from the linear regression of the evolutions of NL^{Si} *vs. t* reported in Figure 1.

Glass	SBN	SBNFe
r_0 (10^{-2} g.m^{-2}.d^{-1})	15 ± 2	2.6 ± 0.3

3.2. Long-term experiments

3.2.1. Characterization of the alteration layer

3.2.1.1. Morphology and composition

The SEM cross-sectional observations and the GD-OES or ToF-SIMS depth elemental profiles carried out on glass monoliths altered for 323 days are shown in Figures 4 and 5 respectively. The thicknesses of the alteration layers formed during long-term experiments were also estimated from SEM cross-sectional images and/or elemental profiles. All these estimates are collected in Table 3, where they are compared to the equivalent altered glass thicknesses L_{AG}^{eq} determined according to Eq. (4) from the data of solution analyses reported in subsection 3.2.2.

The alteration layer was not observed by SEM for monoliths altered during the (SBN; H_2O) experiment (Figure 4a), suggesting it is too thin to be observed by this method. This assumption is supported by the GD-OES elemental profiles recorded for a monolith altered in similar conditions. In spite of the poor depth resolution of these GD-OES profiles (likely a consequence of a too high imposed discharge power of 40 W), the variations of the B signal allow to estimate the thickness of this alteration layer to about 20 nm (Table 3).

The SEM observations performed after the (SBNFe; H_2O) experiment are shown in Figures 4b, 4e and 4h. A single alteration layer with a thickness of ≈300 nm is observed (Table 3). This differs from the systematic observation of a double layer for monoliths altered in the $FeCl_2$ solution, *i.e.* (SBN; $FeCl_2$) experiment (Figures 4c, 4f and 4i) or (SBNFe; $FeCl_2$) experiment (Figures 4d, 4g and 4j). This double layer is made of an inner layer (in contact with the pristine glass) and an outer one designated by "α" and "β" respectively in Figure 4 and in the following. Layer β generally appears more "grainy" than layer α (Figures 4d, 4i and 4j), which could mean that it is made up of nanometric crystallites. The thicknesses of these two layers estimated from SEM observations are given in Table 3. It can be noticed that the alteration layer can locally peel off from the surface of the pristine glass (Figures 4f and 4g), which seems to be the consequence of sample manipulations. In addition, "holes" are present in different proportions in Figures 4e, 4f and 4g. Their origin has not been understood yet.

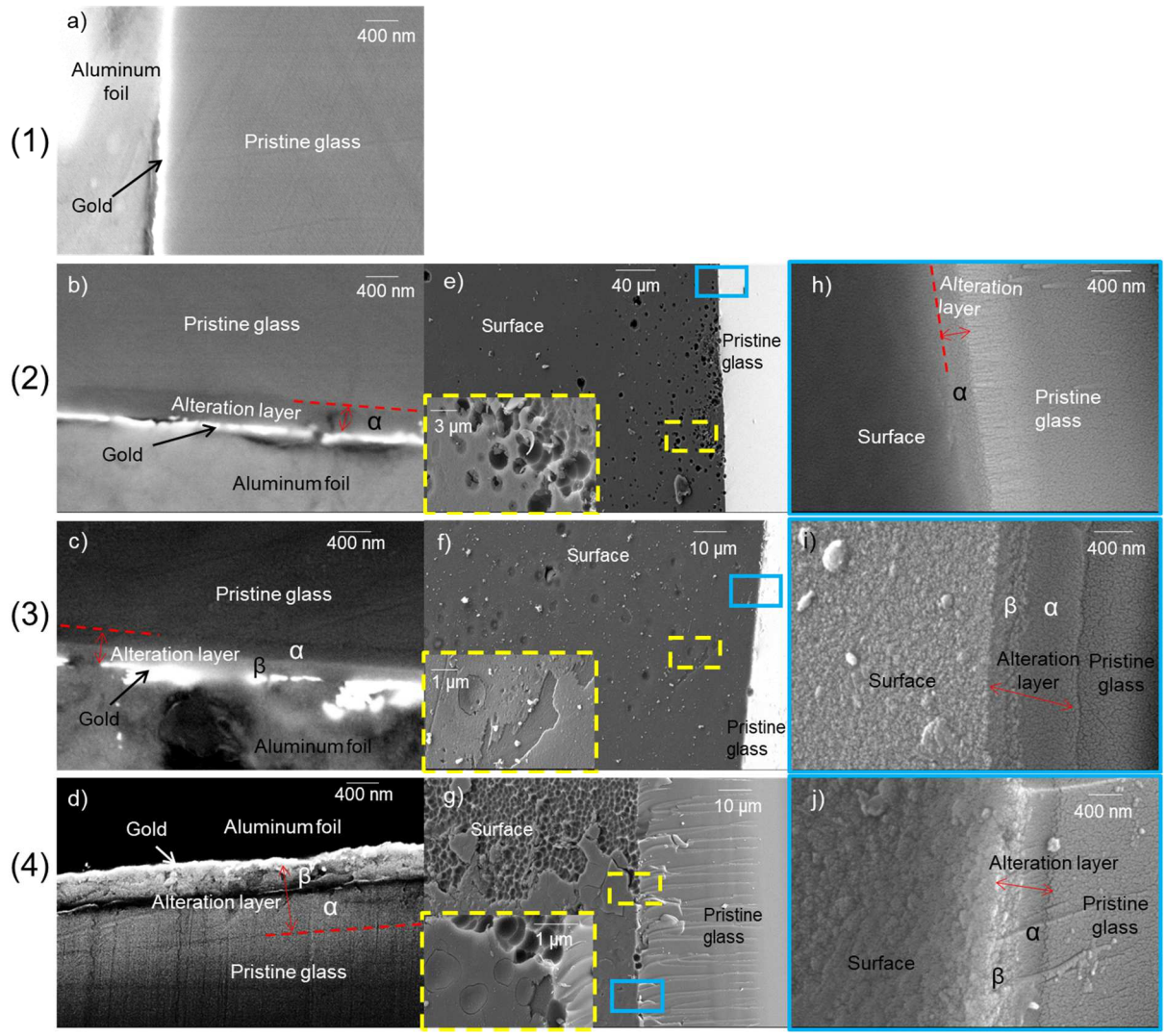

Figure 4. SEM images of monoliths altered at 50°C and free pH during 323 days (S/V = 20 000 m^{-1}); (1), (2), (3) and (4) correspond respectively to (SBN; H_2O), (SBNFe; H_2O), (SBN; $FeCl_2$) and (SBNFe; $FeCl_2$) experiments. Observations were performed on polished cross sections (a-d), on fractured cross sections (e-g; insets correspond to observations at higher magnifications of the zones framed in yellow dotted lines) and on fractured cross sections zooming on the alteration layer / pristine glass interface (h-j; images corresponding to areas framed in blue lines on images e) to g) respectively).

Figure 5 shows GD-OES and/or ToF-SIMS depth profiles collected on monoliths taken at the end of (SBNFe; $FeCl_2$), (SBNFe; H_2O) and (SBN; $FeCl_2$) experiments.

The GD-OES profiles recorded on the altered (SBNFe; $FeCl_2$) monolith (Figure 5a) reveal three successive zones. The first one corresponds to pristine glass with matching Si, B, Na and Fe contents. An inner alteration layer (layer α) is then observed, characterized by (i) an increase of Si (to about 70 at.% of the analyzed elements[5]) and Fe contents and (ii) high depletions in B and Na (both down to about 5 at.%) with respect to pristine glass. This composition in Si, B and Na [25, 34] identifies this layer as the alteration gel [6]. The outer layer (layer β) is strongly enriched in Fe (up to 47 at.%) and depleted in Si (down to about 45 at.%) and Na compared to layer α; the boron content does not seem to change much between the two layers. The high Fe and Si contents in layer β hint at the presence of Fe-

[5] Note that all the contents expressed in at.% in the rest of this work are normalized with respect to the sum of Si, B, Na and Fe contents.

390 silicate. These findings agree well with SEM observations (Figures 4d and 4j), which show the formation of a double alteration layer. The "granular" appearance of layer β (Figures 4d and 4j) is also consistent with presence of Fe-silicate crystals. In order to evaluate the thicknesses of layers α and β from GD-OES profiles, the localization of the pristine glass / layer α interface has been estimated from the half variation of the boron signal between the
395 pristine glass and layer α. Likewise, the localization of the layer α / layer β interface has been estimated from the half variation of Fe signal between the two layers[6]. The resulting thicknesses are given in Table 3. It can also be noticed that the Fe content in layer α decreases continuously from the layer β / layer α interface to the layer α / pristine glass interface. This observation suggests that Fe cations originating from the $FeCl_2$ supernatant
400 can diffuse through the gel layer formed on the SBNFe surface.

ToF-SIMS profiles have been recorded on a second monolith from the same experiment (Figure 5b). The comparison of Figures 5a and 5b reveals a fairly good agreement between results obtained by GD-OES and ToF-SIMS, either in terms of layer thicknesses (Table 3) or evolution of the elemental profiles through the layer α and the pristine glass. Some
405 differences are however observed in terms of element contents (compare for example the average Si content in the layer α which can be around 70 at.% or 80 at.% depending on whether the profile was acquired by GD-OES or ToF-SIMS). On the other hand, significant discrepancy is observed between Na profiles recorded in layer β. This shows that the quantification method applied to ToF-SIMS profiles leads to reliable values in pristine glass
410 and in layer α, but not in layer β. As previously discussed, layer α seems to correspond to the alteration gel while the layer β seems to consist of crystalized Fe-silicate. The comparison between GD-OES and ToF-SIMS quantified profiles thus suggests that the ionization yield of the analyzed species changes little whether they are emitted from the gel or from the glass. This is probably the consequence of only moderate structural differences
415 between the silicate network of the pristine glass and the gel formed under experimental conditions investigated here. On the other hand, it is likely that the ionization yields of the species emitted from crystalline or amorphous phases are different, which precludes quantification of ToF-SIMS data recorded in the Fe-silicate layer using a method based on glass standards (see subsection 2.4).

420 The ToF-SIMS profiles recorded on the (SBNFe; H_2O) monolith are shown in Figure 5c. These profiles hint at a single layer, which is consistent with SEM observations (Figures 4b and 4h). This layer is expected to be the alteration gel as discussed in subsection 3.2.1.2 from XRD results. The ToF-SIMS profiles shown in Figure 5c can then be considered as semi-quantitative. These profiles show that the alteration layer is very rich in Si (more than
425 80 at.%), contains only a small amount of boron (about 2 at.%), and is highly depleted in Na compared to pristine glass. All these features support the hypothesis that this layer is the alteration gel. It can also be noticed that this layer contains Fe and Na in equivalent proportions (about 7 at.%). The measured $\frac{\mathrm{Fe}}{\mathrm{Na}}$ atomic ratio equals 0.98 ± 0.04 on average over the entire layer. This ratio is much lower than those generally observed in Fe-silicates,
430 which typically range from 3 to 28 [16, 35], and so it cannot result from local precipitation of Fe-silicate inside the gel. On the other hand, this $\frac{\mathrm{Fe}}{\mathrm{Na}}$ ratio can be explained by considering

[6] Note that the same method has been applied to delimitate pristine glass / layer α and layer α / layer β interfaces for all the depth elemental profiles reported in this work.

that Fe^{3+} cation is incorporated into the gel structure as $[FeO_{4/2}]^-$ tetrahedral units, resulting in a charge deficit balanced by a Na^+ ion. Therefore, this result suggests that Fe^{3+} cations released during SBNFe alteration into initially pure water are incorporated into the gel with the same coordination than in the pristine glass structure. This kind of result has already been observed for SON68 glass leached in contact with an iron foil and Callovo-Oxfordian clay at 90 °C [36].

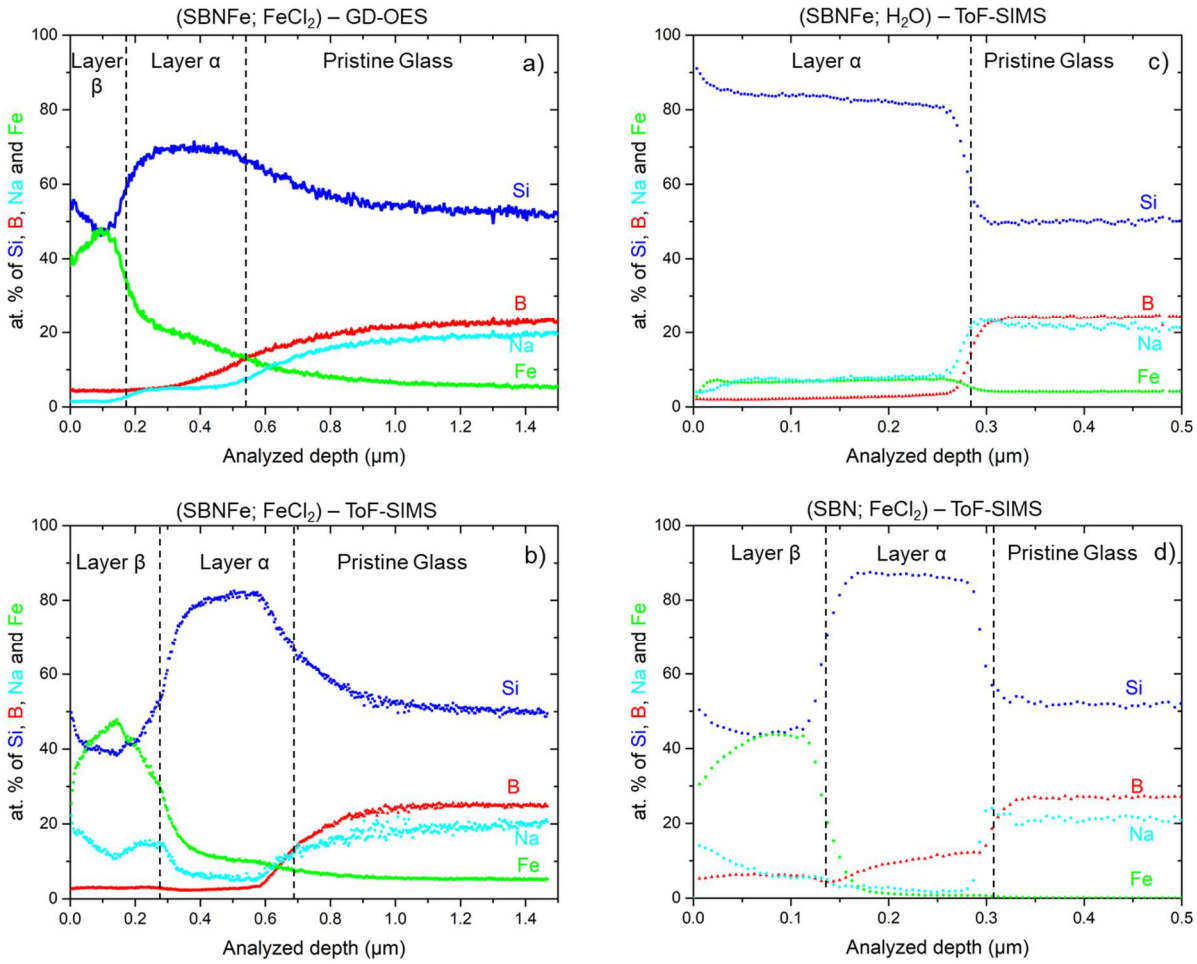

Figure 5. Si, B, Na and Fe depth profiles (in at.% normalized with respect to the sum of Si, B, Na and Fe contents) recorded on monoliths altered at 50°C and free pH during 323 days (S/V = 20 000 m^{-1}). a) GD-OES profiles recorded on sample from (SBNFe; $FeCl_2$) experiment. b-d) ToF-SIMS profiles recorded on samples from (SBNFe; $FeCl_2$), (SBNFe; H_2O) and (SBN; $FeCl_2$) experiments, respectively. Black dotted lines delineate the interfaces between successive layers.

The ToF-SIMS profiles measured on the (SBN; $FeCl_2$) monolith (Figure 5d) are quite similar to that recorded on the (SBNFe; $FeCl_2$) one (Figure 5b). As in all profiles previously described, layer α is both enriched in Si (up to almost 90 at.% of analyzed elements) and depleted in Na and B, which seems to be characteristic of the alteration gel [25, 34]. Although ToF-SIMS profiles cannot be considered quantitative in layer β, the qualitative evolution of Fe, Na, B and Si signals in this layer is close to that observed in Figure 5b. It is therefore possible to conclude that layer β is made of similar Fe-silicates in both long-term experiments in $FeCl_2$ solution. It can however be noted that the gel formed on the surface of the (SBN; $FeCl_2$) sample is almost free of Fe (Figure 5d), as opposed to the (SBNFe; $FeCl_2$) sample (Figure 5b). This comparison suggests that the gel formed on the Fe-free glass is a better “diffusion barrier” than that formed on the Fe-containing glass, at least with respect to

ingress of Fe cations from the $FeCl_2$ supernatant. Note that the gel formed on SBN is however thinner than that formed on SBNFe (Table 3).

Table 3. Comparison between the equivalent altered glass thicknesses L_{AG}^{eq} (determined according to Eq. (4) on the basis of solution analyses) and alteration layer thicknesses estimated from SEM observations (carried out on polished cross sections) and from GD-OES and ToF-SIMS profiles performed on monoliths altered at 50°C and free pH during 323 days (S/V = 20 000 m^{-1}).

Methods	Thicknesses (nm)	Experiments			
		(SBN; H_2O)	(SBNFe; H_2O)	(SBN; $FeCl_2$)	(SBNFe; $FeCl_2$)
SEM	L_β[a]	*no*[b]	*no*	200	340
	L_α[a]	*no*	300	200	490
	L_T[a]	*no*	300	400	830
GD-OES	L_β	*um*[b]	*na*	*na*	190
	L_α	*um*	*na*	*na*	370
	L_T	≈20	*na*	*na*	560
ToF-SIMS	L_β	*na*[b]	*no*	140	270
	L_α	*na*	280	160	420
	L_T	*na*	280	300	690
Solution analyses	L_{AG}^{eq}	290 ± 40	400 ± 70	530 ± 70	830 ± 150

[a] L_α, L_β and $L_T = L_\alpha + L_\beta$ refer respectively to the thickness of the layer α, the thickness of the layer β and the total alteration layer thickness estimated from the characterization of the monoliths.

[b] The notations *um*, *na* and *no* mean unmeasurable, not analyzed and not observed, respectively.

SEM observations coupled with EDX analyses were also performed in an area of the (SBN; $FeCl_2$) monolith where the alteration layer had flaked off (Figure 6). Flaking of the alteration layer made it possible to observe layers α and β separately *via* a top view (Figure 6a). EDX spectra could thus be recorded on each of the two sublayers, as well as on the underlying pristine glass (Figure 6b), as shown schematically in Figure 6c. One limitation of this approach is that the interaction depth of the SEM probe is larger than the thicknesses of layers α and β (see Table 3), which precludes individual analysis of each layer by EDX. Still, EDX spectra (Figure 6b) can be used to confirm the presence or absence of Fe in each of the two layers. No Fe is observed for the EDX spectrum recorded on pristine glass (Figure 6, Spot 1), as expected from the composition of SBN (Table 1). The EDX spectrum corresponding to Spot 2 in Figure 6 contains the contributions from both layer α and the underlying pristine glass. A weak Fe signal barely above the background noise is observed. The spectrum collected on the upper part of layer α (Figure 6, Spot 3) shows an increase in Fe signal compared to that of Spot 2. Note however that the presence of residues from the layer β on the surface of layer α cannot be excluded, which could explain this significant Fe signal for Spot 3, at least partially. Finally, the EDX spectrum collected on the topmost

alteration layer (Figure 6; Spot 4), containing the contributions from layer α, layer β and pristine glass, shows the most intense Fe signal. These EDX analyses corroborate the scarcity of Fe in layer α (except possibly in the vicinity of the interface between layers α and β) and its presence within layer β, in good agreement with ToF-SIMS profiles (Figure 5d).

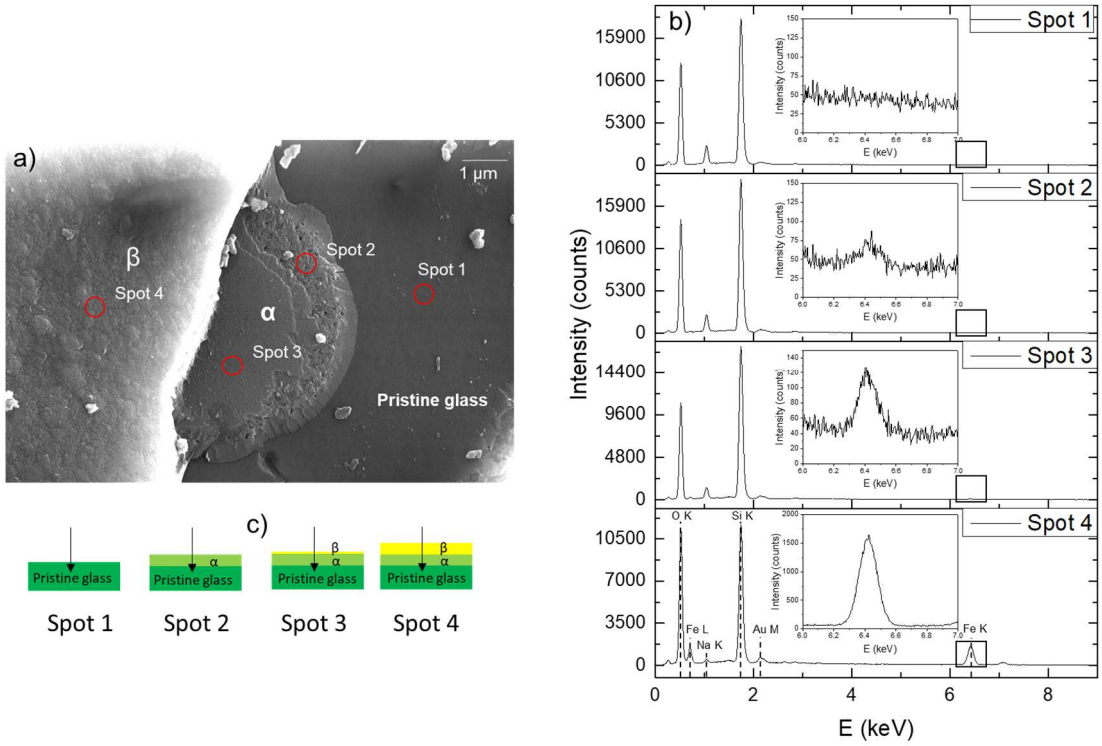

Figure 6. a) SEM direct observation of the surface of the monolith altered during the (SBN; $FeCl_2$) experiment in a zone where the alteration layer has flaked off. b) EDX spectra (each inset corresponds to a zoom on the 6-7 keV range) associated to the four spots marked by red circles on the image a). c) Sketch of the different layers analyzed by EDX.

3.2.1.2. Nature of secondary phases

Figure 7 compares the results of XRD analyses performed on pristine SBNFe and on samples from (SBNFe; H_2O), (SBN; $FeCl_2$) and (SBNFe; $FeCl_2$) experiments.

The XRD patterns recorded on pristine SBNFe and on the altered glass powder from the (SBNFe; H_2O) experiment are quite similar (Figure 7a). They are both typical of amorphous phases [37], suggesting that the alteration layer formed during the (SBNFe; H_2O) experiment does not contain crystalized phases in amounts high enough to be detected by XRD. This is consistent with the composition of this layer, which exhibits Si enrichment coupled with B and Na depletions with respect to pristine glass (see subsection 3.2.1.1 for details). Indeed, these composition features are characteristic of amorphous gel formed during leaching of such simple glasses [25, 34]. Note that layers α for all samples share these compositional features. It therefore seems reasonable to conclude that all of these layers correspond to an amorphous gel, *i.e.* the alteration gel [6, 25, 34].

In addition to the signal associated to amorphous phases, two peaks are present on the XRD pattern recorded on the (SBNFe; $FeCl_2$) glass powder (Figure 7b). The first one, corresponding to an interplanar spacing *d* of about 1.54 Å, is conspicuous, whereas the

second one at *d* value of approximatively 2.57 Å partially overlaps with the main amorphous bump. According to Thien *et al.* [38] these two peaks are diagnostic of the formation of trioctahedral smectite, with $d \approx 1.54$ Å corresponding to the (060) reflection [16, 38-39]. Nevertheless, it should be noted that the (001) basal reflection, resulting from the stacking of smectite layers [39], cannot be observed in the investigated *d* range[7]. Nevertheless, it seems reasonable to conclude that layer β formed during the (SBNFe; $FeCl_2$) experiment is made of trioctahedral smectite considering: (i) its composition which is typical of a Fe-silicate, and (ii) the presence of the *d*(060) reflection close to the position expected for trioctahedral smectites [39]. Note that a Fe-rich trioctahedral smectite is also the secondary phase formed on another simple borosilicate glass leached in $FeCl_2$ solution in the same conditions [16].

The reflections at 1.54 Å and 2.57 Å are also observed on the XRD patterns recorded on altered glass powder (Figure 7b) and on the precipitates recovered on a cellulose acetate filter (Figure 7c), both taken from (SBN; $FeCl_2$) experiment. The reflection at 2.57 Å is even more easily identifiable on the filtered precipitate (Figure 7c) as the sample is free of glass and alteration gel. The XRD results in Figures 7b and 7c therefore make it possible to conclude that whatever the glass studied here, the same crystallized secondary phase, a trioctahedral smectite, is formed during leaching in $FeCl_2$ solution.

Other peaks are observed in Figure 7c. They correspond to cellulose acetate, to the silicon (JCPDS file #03-0101) sample holder used for grazing incidence analysis, and to NaCl (JCPDS file #02-8948) precipitating during drying of the unrinsed sample (see subsection 2.2). NaCl was also observed on the XRD pattern recorded on the (SBN; $FeCl_2$) glass powder (Figure 7b) although this sample was rinsed. Rinsing was certainly insufficient to prevent formation of NaCl during drying. This has already been observed in the case of solid samples taken after the alteration of a borosilicate glass in $MgCl_2$ solution [40].

XRD results in Figure 7 thus seem to show that a trioctahedral smectite formed during alteration in $FeCl_2$ solution. Whatever the altered glass, the outer layer formed during alteration in $FeCl_2$ solution consists of Fe-silicates with similar compositions (see subsection 3.2.1.1). The quantitative data obtained by GD-OES on the outer layer for the (SBNFe; $FeCl_2$) monolith (Figure 5a) can therefore be considered as representative of the composition of the trioctahedral smectite formed in this study. The mean $\frac{Si}{Na}$, $\frac{Si}{B}$ and $\frac{Si}{Fe}$ content ratios in the outer layer (layer β) were derived from the integral of Si, Fe and Na signals over the entire thickness of this layer. These ratios are approximately 29.9, 12.2 and 1.23 respectively, which is rather consistent with the composition of phyllosilicates formed by alteration of International Simple Glass (ISG) in the same conditions [16].

It is well known that Si fills tetrahedral sites in smectites, whereas Fe, whether in the +II or +III oxidation state, is preferentially incorporated in octahedral sheets [16, 39, 41]. Iron can nevertheless fill a tetrahedral position when the total amount of Fe is high [39], as is the case here (the $\frac{Si}{Fe}$ ratio is about 1.23). Sodium can be incorporated into smectites as an interlayer cation [16, 38-40], while B can occupy a tetrahedral position [42-43] or be incorporated as $B(OH)_3$ into the interlayer [44] in clay minerals. Based on these considerations and on the

[7] Indeed, the *d*(001) value is typically greater than 10 Å for trioctahedral smectites formed during the leaching of borosilicate glasses under conditions close [38] or identical [16] to those studied here.

general chemical formula for 2:1 trioctahedral phyllosilicates [16], a generic chemical formula can be proposed for Fe-rich trioctahedral smectite formed in this study:

$$[\mathrm{Na}_{y+z-v},(\mathrm{B(OH)_3})_x](\mathrm{Si}_{4-(y+z)}\mathrm{B}_y\mathrm{Fe}^{3+}_z)(\mathrm{Fe}^{2+}_{3-v}\mathrm{Fe}^{3+}_v)\mathrm{O}_{10}(\mathrm{OH})_2 \quad (6).$$

The respective values of *x*, *y*, *z* and *v* cannot be determined on the basis of only three content ratios (*i.e.* $\frac{\mathrm{Si}}{\mathrm{Na}}$, $\frac{\mathrm{Si}}{\mathrm{B}}$ and $\frac{\mathrm{Si}}{\mathrm{Fe}}$). It is therefore not possible to establish the exact composition of the trioctahedral smectite formed in this work, but the compositional range can be bounded by considering two limit cases. If B fills only tetrahedral sites, then the composition of the smectite can be defined as:

$$[\mathrm{Na}_{0.12}](\mathrm{Si}_{3.70}\mathrm{B}_{0.30})(\mathrm{Fe}^{2+}_{2.82}\mathrm{Fe}^{3+}_{0.18})\mathrm{O}_{10}(\mathrm{OH})_2 \quad (7).$$

Therefore, Fe is only incorporated into the octahedral sheets; mainly as Fe^{2+}. If it is instead assumed that B is fully incorporated as $B(OH)_3$ into the interlayer, this composition becomes:

$$[\mathrm{Na}_{0.13}(B(OH)_3)_{0.32}](\mathrm{Si}_{3.86}\mathrm{Fe}^{3+}_{0.14})(\mathrm{Fe}^{2+}_{2.99}\mathrm{Fe}^{3+}_{0.01})\mathrm{O}_{10}(\mathrm{OH})_2 \quad (8).$$

Hence, some Fe fills tetrahedral sites. In this case, octahedral sites are almost exclusively filled by Fe^{2+} cations. The $\frac{\mathrm{Fe}^{2+}}{\mathrm{Fe}^{2+}+\mathrm{Fe}^{3+}}$ content ratios derived from chemical formulas (7) and (8) are approximately 0.94 and 0.95, respectively. This indicates that whatever the exact composition of the trioctahedral smectite formed in this study, Fe is mainly incorporated in the +II oxidation state. Furthermore, Wilson *et al.* [41] have shown that the *d*(060) value depends on the oxidation state of Fe in Fe-rich trioctahedral smectite. A *d*(060) value of around 1.54 Å as observed in Figure 7 could thus reflect a mixture of Fe^{2+} and Fe^{3+} in the octahedral sheets [41]. This is in agreement with a composition of the trioctahedral smectite formed in this study between the boundaries defined by formulas (7) and (8).

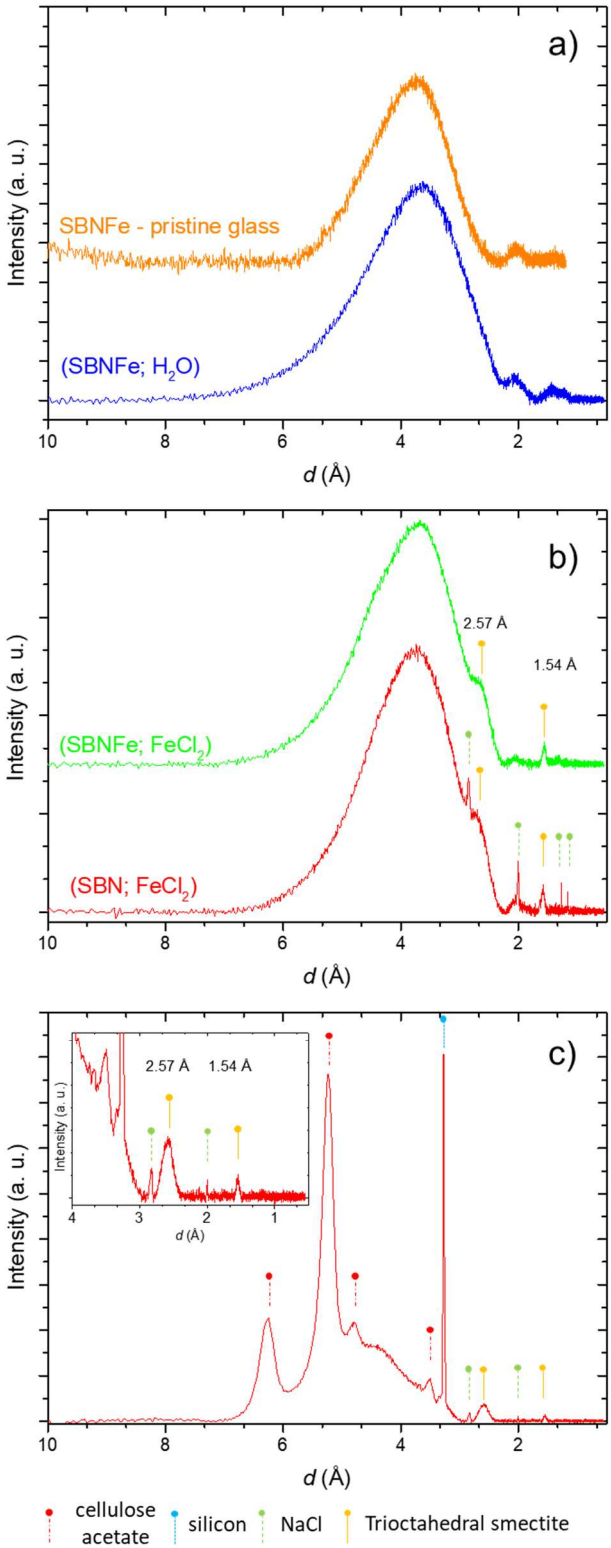

Figure 7. XRD patterns for samples leached at 50°C and free pH for 323 days (S/V = 20 000 m^{-1}). a) Comparison of patterns recorded on altered glass powder from (SBNFe; H_2O) experiment and on pristine SBNFe powder. b) Comparison of patterns recorded on altered glass powders from (SBN; $FeCl_2$) and (SBNFe; $FeCl_2$) experiments. c) Precipitates collected on a cellulose acetate filter by vacuum filtration of the leaching solution from the (SBN; $FeCl_2$) experiment (the inset corresponds to a zoom on the 0.5-4 Å range). The notation *d* refers to the interplanar spacing.

3.2.1.3. Summary of key Findings

Whatever the glass considered, the layer formed during leaching in initially pure water seems to be made only of the alteration gel [6]. This seems well established for altered SBNFe samples. Some uncertainty still subsists in the case of SBN due to the thinness of the alteration layer, but the validity of this conclusion is supported by the SBN composition (see Table 1). In addition, it is corroborated by results showing that only silica gel forms on the surface of the same glass when it is leached into initially pure water [34].

The leaching of SBN and SBNFe in the $FeCl_2$ solution systematically leads to the formation of a double alteration layer. The inner part of this layer seems to be made of a gel, and the outer part of crystallized Fe-silicates. These silicates seem similar in terms of composition or crystallographic structure regardless of the glass studied. They correspond to Fe-rich trioctahedral smectites, in agreement with previous results on the alteration of ISG under conditions identical to those studied here [16]. The composition of the Fe-rich trioctahedral smectite falls in the range bounded by chemical formulas (7) and (8). It incorporates of course a large amount of Fe ($\frac{Si}{Fe}$ ratio about 1.23), mainly in the +II oxidation state; but also a small amount of B ($\frac{Si}{B}$ ratio about 12.2).

Composition profiles measured in this study have shown that a small amount of B is retained in the alteration gel (see Figure 5). Even if B seems to be the best tracer for studying the alteration kinetics of this type of glass during long-term experiments [25, 27], it should be kept in mind that a small amount of B can be retained in the alteration products.

All the gel layers characterized in this study share the same three compositional features: they are enriched in Si (the Si content varies from 70 at.% to 90 at.% with respect to the sum of Si, B, Na and Fe contents) and depleted in B and Na with respect to pristine glass. This is in good agreement with the known properties of amorphous gel formed during leaching of this type of simple glass [25, 34]. Note that the gel composition also depends on the underlying glass as well as on the leaching medium. Thus, in the case of SBNFe leached in initially pure water, Fe^{3+} cations released during glass alteration seem to be incorporated into the gel structure as tetrahedral $[FeO_{4/2}]^-$ units balanced by Na^+ ions. When the same glass is leached in the $FeCl_2$ solution, Fe cations from the supernatant seem to diffuse through the gel layer (see Figure 5). Conversely, it can be noted that the gel formed on the surface of SBN leached in the $FeCl_2$ solution (layer α) is almost free of Fe (Figure 5). This difference suggests that the gel formed on the surface of the Fe-free glass is a better “diffusion barrier” than that formed on the surface of the Fe-containing glass. This seems to be the case at least for the ingress of Fe cations from the $FeCl_2$ supernatant. However, it now seems well established in the literature that the ingress of water through the gel layer involves a pore network [6, 26]. The diffusion of Fe cations from the supernatant could thus be a tracer of the ingress of water within the gel and provide information on its passivating properties.

The thicknesses of all the alteration layers characterized in this work were estimated from elemental profiles or SEM images (Table 3). These results obtained by independent techniques are rather consistent. The observed differences can originate from the specific features of each of the three methods used, or from local variations in the alteration layer thickness. Note for example that the area analyzed by GD-OES has a diameter of 4 mm

while the dimensions of that analyzed by ToF–SIMS are limited to a 50×50 µm² (see subsection 2.4).

Nevertheless, the data collected in Table 3 show that whatever the glass considered, the alteration layer (but also probably the gel) formed after 323 days in the $FeCl_2$ solution is always thicker than that formed in initially pure water for the same duration. Moreover, these data seem to highlight that whatever the leaching solution, the gel formed on the surface of the Fe-containing glass is always thicker than that formed on the surface of the Fe-free glass.

3.2.2. Leaching kinetics

The Figure 8 shows the time-dependent evolution of NL^i, [Si] and pH values measured in the leaching solutions during long-term alteration experiments.

The evolutions of NL^i (in which *i* refers to B, Na, Si or Fe in the case of the (SBNFe; H_2O) experiment) for experiments carried out in initially pure water are presented in Figure 8a. In the case of (SBN; H_2O) experiment, B and Na are released congruently while Si is mainly retained in the alteration gel. A rapid increase of both NL^{B} and NL^{Na} values is observed over the first 50 days or so. The alteration rate drastically decreases over longer durations, leading to normalized mass losses that no longer progress significantly. Throughout the duration of the (SBN; H_2O) experiment, the pH remained almost constant (Figure 8d), with an average value of approximately 9.4. at 50 °C. After one day of reaction, [Si] also seems to remain approximately constant (≈7.0 mmol.L^{-1} on average) until the end of the experiment (Figure 8c). The drop in the alteration rate, indicated by both evolutions of NL^{B} and NL^{Na} between 1 and ≈60 days of reaction (Figure 8a), therefore cannot be attributed to a decrease in the hydrolysis reaction affinity with respect to silicic acid species in this case. Rather it would correspond to the formation of a passivating gel at the glass surface, in agreement with previous studies [34]. In addition, the value of about 7 mmol.L^{-1} corresponds to the solubility of amorphous silica at pH = 9.4, based on data published by Fleming & Crerar [45] using the ionization constant of water at 50 °C calculated from Bandura & Lvov [46]. This is also consistent with previous report of the formation of a silica gel during leaching of the same glass in initially pure water [34].

The formation of a silica gel during (SBN; H_2O) experiment is in agreement with NL^{Si} values showing that Si is mainly retained in the alteration layer (Figure 8a). From the value of L_{AG}^{eq} estimated from solution analyses (≈290 nm, see Table 3), it seems that the thickness of the gel formed during the (SBN; H_2O) experiment was underestimated from characterization results (at most ≈20 nm; Table 3). The reason for this has not been clearly understood yet. An overall peeling of the layer formed on monoliths altered during the (SBN; H_2O) experiment might have occurred during sample manipulations before solid characterizations.

In the case of (SBNFe; H_2O) experiment, B and Na are released in significant amounts, but NL^{B} is always higher than NL^{Na} (Figure 8a). This incongruence between B and Na implies that Na^+ is retained in the alteration layer, in agreement with depth elemental profiles (Figure 5c). Furthermore, Si and Fe are strongly retained within the gel. It is interesting to note that the alteration rate of SBNFe is lower than that of SBN during the first days of leaching (Figure 8a). This is in agreement with strengthening of the glass network against hydrolysis reactions by tetrahedrally coordinated Fe^{3+}, as shown in subsection 3.1. However, the

alteration rate of SBNFe decreases more slowly than that of SBN, so that SBNFe leaches the fastest after ≈60 days of reaction. After 323 days of leaching in initially pure water, SBNFe is thus significantly more altered than SBN, as shown by the values of the altered glass fraction $f_{AG}^{\mathrm{B}}(t_f)$ (Table 4) or of L_{AG}^{eq} (Table 3) determined at the end of the experiments. As in the case of (SBN; H_2O) experiment, the pH remained approximately constant and close to 9.2 on average during the experiment (Figure 8d). The [Si] values also stabilized fairly close to the solubility of amorphous silica at pH = 9.2 [45], but only after about 90 days of leaching (Figure 8c).

It can also be noted in Figure 8a that NL^{Si} measured during the alteration of both SBN and SBNFe in initially pure water remain similar throughout the duration of the experiments. In both cases, the NL^{Si} values are very low which indicates that almost all of the Si released during glass alteration is incorporated into the gel. On the other hand, the NL^{B} curves show that SBNFe is more altered than SBN after ≈90 days of leaching. From this moment, the gel formed on SBNFe therefore becomes thicker than that formed on SBN. Although thicker, this gel is less passivating since SBNFe is the most altered glass after 323 days (Table 4).

Figure 8b shows the evolution of NL^{i} values for experiments in the $FeCl_2$ solution. The observed trends are quite similar to those observed in initially pure water (Figure 8a), but with some delays in time. For both experiments, Si is mainly retained in the alteration layer. The experiment carried out on SBN leads to a congruent release of B and Na. This release is characterized by a first phase of rapid increase in NL^{B} and NL^{Na} before a plateau reached after ≈120 days of leaching, compared to ≈60 days for (SBN, H_2O) experiment (Figure 8a). In addition, as in the case of experiments in initially pure water, the alteration rate of SBN is initially higher, but later decrease more rapidly than that of SBNFe, so that SBNFe is more altered than SBN after about 175 days of leaching. The same switch in reaction amplitude is thus observed in both media, although it occurs later in the $FeCl_2$ solution.

On the other hand, it can be noticed that B and Na are released congruently during SBNFe leaching in the $FeCl_2$ solution (Figure 8b), contrary to what was observed for the (SBNFe; H_2O) experiment. It is also important to note that the glasses are generally altered faster in the $FeCl_2$ solution, which results in higher $f_{AG}^{\mathrm{B}}(t_f)$ (Table 4) and L_{AG}^{eq} (Table 3) values than at the end of experiments in initially pure water. The pH measured in $FeCl_2$ leaching solutions are also very different from those measured for experiments in initially pure water (Figure 8d). With the exception of values measured around 60 days for (SBN; $FeCl_2$) experiment (which will be discussed later), the pH remained roughly constant, between 6.1 and 6.3 on average. After one day of reaction, [Si] (Figure 8c) seems to remain approximately constant in both experiments (about 2.9 $mmol.L^{-1}$ on average), once again, rather close to that of the solubility of amorphous silica at the pH of experiments [45].

The fact that NL^{B} and NL^{Na} reach a plateau after approximately 120 days of reaction in the (SBN; $FeCl_2$) experiment (Figure 8b), without significant variations in [Si] over this period (Figure 8c), shows that a strongly passivating gel (leading to a rate drop by a factor of ≈14 between 1 and 148 days of leaching) has formed on the surface of SBN during its alteration in the $FeCl_2$ solution. This result is consistent with depth elemental profiles (Figure 5d), which show that Fe cations from the $FeCl_2$ supernatant hardly penetrates inside the gel formed during the (SBN; $FeCl_2$) experiment. This formation of a strongly passivating gel contrasts with previous observations suggesting that the presence of Fe in the medium prevents the

formation of a protective gel [15-17, 36, 47] and keeps glass alteration at a high rate over a long period of time [14-15, 36, 48] (in any event significantly longer than investigated here). This phenomenon is generally attributed to the precipitation of Fe-silicates [14-17, 36, 47, 49].

In the case of (SBN; $FeCl_2$) experiment, the formation of a passivating gel occurs jointly with precipitation of Fe-silicates, as shown by characterizations of solid alteration products. The time-dependent evolution of the amount of Fe cations consumed from the supernatant (n_{Fe}^{c}) during the (SBN; $FeCl_2$) experiment is shown in Figure 9a (where n_{Fe}^{c} is normalized to S_G to allow comparison between the results of the two experiments carried out in $FeCl_2$ solution). This Fe uptake can be attributed to the precipitation of Fe-silicates during the (SBN; $FeCl_2$) experiment, whether on the surface of the gel or as precipitates in the leaching solution. The ratio between the amount of B released in the supernatant during glass alteration and n_{Fe}^{c} ($n_{\mathrm{B}}^{rel}/n_{\mathrm{Fe}}^{c}$) can be plotted as a function of time (Figure 9b). After a short transient period of about 30 days, the $n_{\mathrm{B}}^{rel}/n_{\mathrm{Fe}}^{c}$ ratio seems to stabilize at an average value of 2.01 ± 0.08, which does not depend on the duration of the (SBN; $FeCl_2$) experiment. This seems to indicate that after ≈30 days of leaching, the glass alteration occurs in the pseudo-steady-state regime [50], during which the ratio between the rate of glass alteration ($\propto \frac{dn_{\mathrm{B}}^{rel}}{dt}$) and that of Fe-silicates precipitation ($\propto \frac{dn_{\mathrm{Fe}}^{c}}{dt}$) is independent of time. Note, however, that Figures 8b and 9a respectively show that $\frac{dn_{\mathrm{B}}^{rel}}{dt}$ ($\propto \frac{dNL^{\mathrm{B}}}{dt}$) and $\frac{dn_{\mathrm{Fe}}^{c}}{dt}$ are time dependent, even when their ratio is not. This suggests that these two rates are actually controlled by the same rate-limiting process, whether related to Fe-silicates precipitation or to the passivating gel formation.

If the limiting process was part of the mechanism of Fe-silicates precipitation, the Fe consumption rate (*i.e.* $\frac{dn_{\mathrm{Fe}}^{c}}{dt}$) should mainly depend on [Fe], since [Si] (Figure 8c) and the pH (except the value measured at ≈60 days, Figure 8d) remain roughly constant once the pseudo-steady-state regime is established (Figure 9b). The comparison of Figures 9a and 9c shows that there is no direct link between the time-dependent evolutions of [Fe] and of $\frac{dn_{\mathrm{Fe}}^{c}}{dt}$. Therefore the rate-limiting process controlling both glass alteration and Fe-silicate precipitation during the (SBN; $FeCl_2$) experiment must be part of the mechanism of passivating gel formation. This is consistent with previous work on the leaching of ISG in $FeCl_2$ solution, which concludes that the rate of glass alteration limits the precipitation of secondary phases [16].

Because precipitation of Fe-silicates does not rate-control the kinetics of SBN alteration in the $FeCl_2$ solution (at least once the pseudo-steady-state regime is established), this precipitation could regulate the aqueous concentration of some species involved in the formation of Fe-silicates, *e.g.* [Si] and/or pH. Aréna *et al.* [16] have shown that the precipitation of silicates resulted in a pH decrease. It therefore seems that pH stabilization between 6.1 and 6.3 in the $FeCl_2$ solution (except for one outlier, Figure 8d) is controlled by the precipitation of Fe-silicates. The comparison of respective evolutions of the pH (Figure 8d) and [Fe] (Figure 9c) during the (SBN; $FeCl_2$) experiment supports this hypothesis. Despite periodic additions of concentrated $FeCl_2$ solution, uptake of Fe cations present in the supernatant was almost complete between 29 and 64 days of leaching (Figure 9c). At the same time, the pH of the (SBN; $FeCl_2$) experiment reach its highest value, *i.e.* 7.5 ± 0.1 after

64 days of reaction (Figure 8d). More generally, the variations in pH and in [Fe] during the (SBN; $FeCl_2$) experiment are anticorrelated over the period ranging from 30 to 100 days approximately. This shows that when [Fe] is too low for quantitative precipitation of Fe-silicates, the evolution of the pH is controlled by the release of B (acting as a borate buffer [51]) and Na resulting from glass alteration. On the other hand, as soon as there is enough Fe cations in the supernatant, precipitation of Fe-silicates controls the evolution of the pH, which then stabilizes between 6.1 and 6.3 (Figure 8d).

As in the case of experiments in initially pure water, the gel formed on SBNFe during leaching in the $FeCl_2$ solution appears to be less passivating than that formed on SBN, since the rate drop between 1 and 148 days of leaching is only a factor of ≈3 in the case of (SBNFe; $FeCl_2$) experiment (compared to about ≈14 in the case of (SBN; $FeCl_2$) experiment). The time-dependent evolution of n_{Fe}^{c}/S_G during the (SBNFe; $FeCl_2$) experiment is compared to that of the (SBN; $FeCl_2$) experiment in Figure 9a. As in the (SBN; $FeCl_2$) experiment, the uptake of Fe occurring during the (SBNFe; $FeCl_2$) experiment seems to be the consequence of Fe-silicates precipitation (i) on the gel surface and (ii) within the leaching solution. However, in the case of (SBNFe; $FeCl_2$) experiment, the Fe-silicate precipitation also seems to take place inside the gel since a diffusion of Fe cations from the $FeCl_2$ supernatant through the gel layer was also observed (*cf.* Figures 5a and 5b). This last hypothesis has already been proposed in previous studies [14-17, 49].

It should however be noted that the amount of Fe consumed by Fe-silicates precipitation during the (SBNFe; $FeCl_2$) experiment, as estimated from Eq. (5), is likely an underestimate. This is because Fe supplied by glass leaching is not taken into account. This approximation nevertheless seems reasonable in the present case. Indeed, the Fe^{3+} cations resulting from the alteration of borosilicate glasses appear to be mainly retained in the alteration layer as shown in Figure 8a and in previous work [21]. Moreover, the $\frac{\mathrm{Fe}^{2+}}{\mathrm{Fe}^{2+}+\mathrm{Fe}^{3+}}$ ratio of about 0.95 obtained for chemical formulas (7) and (8) (see subsection 3.2.1.2 for details) shows that the Fe^{3+} cations are only incorporated in small amounts in the Fe-silicates formed in this study. The Fe^{3+} cations released by SBNFe leaching therefore seem to be mainly incorporated into the gel, possibly as hydrous Fe-oxyhydroxides [20], as discussed in more details in subsection 3.3.

The time-dependent evolutions of $n_{\mathrm{B}}^{rel}/n_{\mathrm{Fe}}^{c}$ ratios are compared in Figure 9b for both experiments in the $FeCl_2$ solution. This comparison reveals the same trend: after a transient period which is longer (around 60 days) in the case of (SBNFe; $FeCl_2$) experiment, the $n_{\mathrm{B}}^{rel}/n_{\mathrm{Fe}}^{c}$ ratio seems to stabilize at a value of 2.3 ± 0.1 on average. Thus, as in the case of (SBN; $FeCl_2$) experiment, a pseudo-steady-state regime is reached for the (SBNFe; $FeCl_2$) experiment, but only after ≈60 days of leaching (compared to ≈30 days for (SBN; $FeCl_2$) experiment). During this regime, the same rate-limiting process seems to control the kinetics of both glass alteration and Fe-silicates precipitation. In order to identify this rate-limiting process, the rate of glass alteration at the beginning of the pseudo-steady-state period was estimated. This was performed by deriving NL^{B} *vs. t* curves (Figure 8b) near 30 and 60 days of reaction for (SBN; $FeCl_2$) and (SBNFe; $FeCl_2$) experiments, respectively. These alteration rates are of the same order of magnitude ($(6.7 \pm 0.9)\times10^{-3}$ g.m^{-2}.d^{-1} and $(8.5 \pm 1.0)\times10^{-3}$ g.m^{-2}.d^{-1}, respectively), which could mean that the same rate-limiting process controls the kinetics in both experiments, at least during the pseudo-steady-state regime. As

790 in the case of (SBN; $FeCl_2$) experiment, the kinetics of SBNFe alteration in the $FeCl_2$ solution therefore does not seem to be rate-controlled by Fe-silicates precipitation, at least during the pseudo-steady-state regime. This last hypothesis is consistent with a control of the pH of the leachate by the precipitation of Fe-silicates, as expected from Figure 8d.

Table 4. Values of $f_{AG}^{B}(t_f)$ calculated according to Eq. (2) and of $I_{AG}^{H_2O}$ and $I_{AG}^{FeCl_2}$ as defined in subsection
795 **3.4; all determined after 323 days of leaching at 50°C and free pH (S/V = 20 000 m^{-1}).**

Experiment	(SBN; H_2O)	(SBNFe; H_2O)	(SBN; $FeCl_2$)	(SBNFe; $FeCl_2$)
$f_{AG}^{B}(t_f)$ (%)	11.1 ± 0.7	15.6 ± 0.9	19.9 ± 1.1	30 ± 2
	$I_{AG}^{H_2O}$		$I_{AG}^{FeCl_2}$	
	1.4 ± 0.1		1.5 ± 0.1	

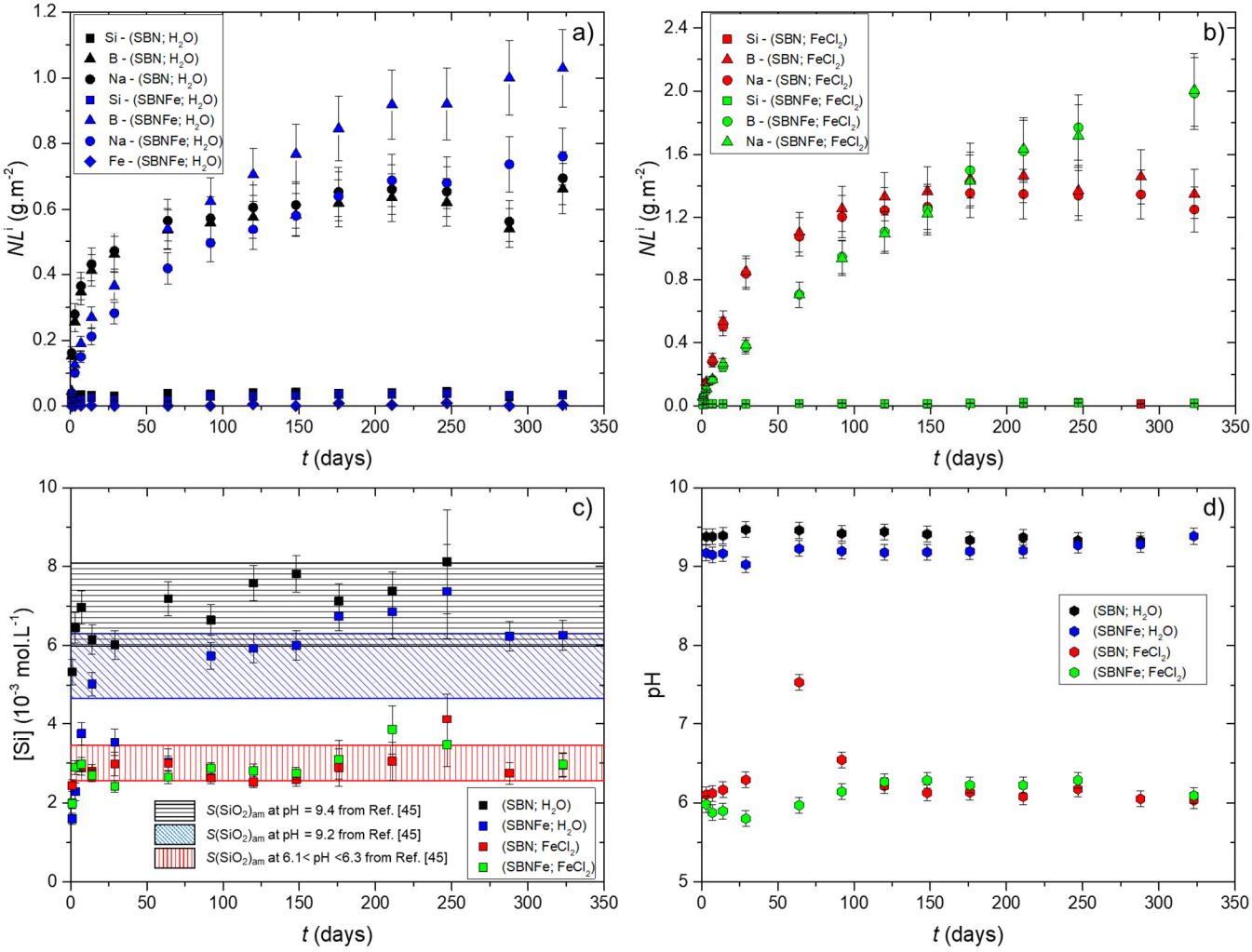

Figure 8. Kinetics data from long-term leaching experiments carried out on SBN and SBNFe at 50°C and free pH during 323 days (S/V = 20 000 m^{-1}). a-b) Evolution of NL^i *vs.* t (in which i refers to B, Na, Si or Fe in
800 **the particular case of the (SBNFe; H_2O) experiment) from experiments performed a) in initially pure water and b) in the 10^{-2} mol.L^{-1} $FeCl_2$ solution. c) Evolution of [Si] in the leachate as a function of time. The notation $S(SiO_2)_{am}$ refers to the solubility of amorphous silica; the values of $S(SiO_2)_{am}$ deduced from Ref.**

[45] are represented by ranges because Fleming & Crerar [45] specify that the relative agreement of their calculations with published data is ± 15%. d) Evolution of pH measured at 50°C as a function of time.

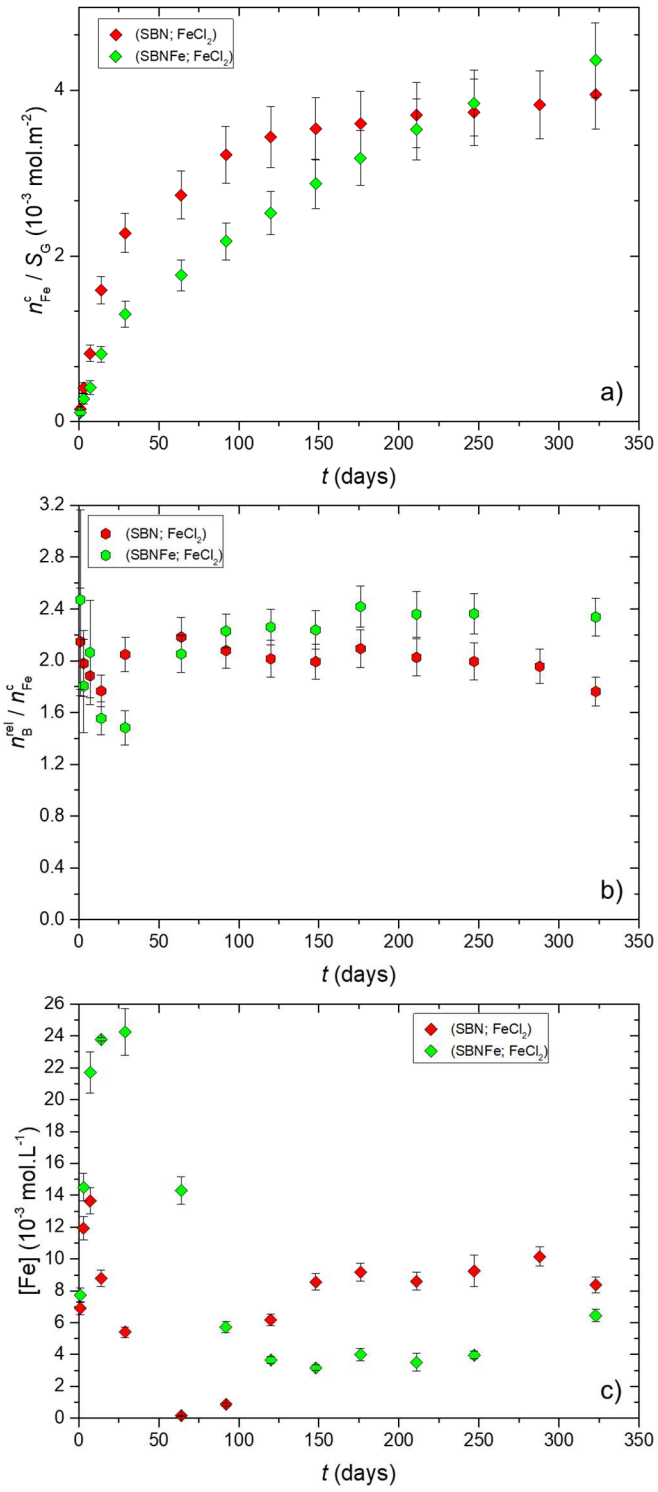

Figure 9. Kinetics data from long-term alteration experiments carried out on SBN and SBNFe in 10^{-2} mol.L^{-1} $FeCl_2$ solution at 50°C and free pH during 323 days (S/V = 20 000 m^{-1}). a) Time evolution of Fe cations uptake (characterized by n^c_{Fe} normalized to S_G to allow comparison between the results of both experiments). b) Time evolution of the n^{rel}_B/n^c_{Fe} ratio. c) Time evolution of [Fe] in the leachate (note that [Fe] never exceeded (2.2 ± 0.4)×10^{-4} mol.L^{-1} during the (SBNFe; H_2O) experiment).

3.3. Gel passivating properties: Fe-containing glass *vs.* Fe-free glass

Whether in initially pure water or in the $FeCl_2$ solution, leaching of SBN during long-term experiments systematically leads to the formation of a highly passivating gel, which causes a drop in the glass alteration rate (Figures 8a and 8b). This phenomenon seems to be attributable to the gel densification over time, caused by recondensation of silicate bonds and leading to clogging of the gel porosity [6, 26]. The gel formed on the surface of SBN thus seems to be a diffusion barrier [6, 34], which strongly limits further glass alteration. This inference is consistent with depth elemental profiles reported in Figure 5d, showing that the gel formed during the (SBN; $FeCl_2$) experiment prevents the ingress of Fe cations from the $FeCl_2$ supernatant.

The alteration rate of SBNFe decreases more slowly than that of SBN during leaching in initially pure water (Figure 8a), suggesting that the gel formed on SBNFe surface is not so passivating than that formed on SBN. This seems to be the consequence of a double effect of Fe^{3+} cations incorporated in the glass structure. On the one hand, Fe^{3+} cations in the glass are present in tetrahedral coordination and charge compensated by Na^+ ions [20, 22]. Therefore, they decrease the number of NBO and strengthen the glass network against hydrolysis reactions. This slows down the build-up of Si in the leaching solution (see Figure 8c), and consequently gel thickening and/or densification. On the other hand, Fe^{3+} incorporated into the gel structure in the same tetrahedral configuration seem to hinder the gel restructuring into a passivating barrier. This last hypothesis, which is analogous to the effect of Al^{3+} incorporated in the glass structure [52], is consistent with the fact that the gel formed on SBNFe in initially pure water is less passivating, albeit thicker, than that formed on SBN.

Digging into this analogy between Fe^{3+} and Al^{3+}, the double effect of Fe present in the glass structure seems to parallel that of Al [21]. Indeed, in the case of simple aluminoborosilicate glasses (SiO_2-B_2O_3-Na_2O-Al_2O_3) leached in initially pure water, it has been shown that Al^{3+} cations are also incorporated in tetrahedral coordination and are charge-compensated by Na^+ ions in the gel structure [53]. Experimental [52] as well as modeling [54] studies about the leaching resistance of this type of glass have shown that increasing amounts of Al in the pristine glasses (from 0 to 5 mol.% of Al_2O_3, *i.e.* over a range similar to that studied here for Fe_2O_3) reduce the initial rate of dissolution but eventually lead to greater alteration extent. The initial effect is the consequence of Al^{3+} incorporation into the pristine glass structure (in a similar way to Fe^{3+} [52-53]), which strengthens the glass network [52, 54]. The later effect is explained by the presence of Al in the gel, which slows down the kinetics of hydrolysis and condensation reactions, hinders the gel reorganization, and eventually delay the formation of a passivating layer [52-53]. Yet, it can be noticed that even if the addition of Al in the glass leads to higher alteration extent, the formation of a strongly passivating layer is ultimately expected [52, 54]. This phenomenon has not been clearly observed in our study, but was observed by Gin *et al.* [22] for a significantly longer experiment (about 2000 days) carried out on a quaternary glass (SiO_2-B_2O_3-Na_2O incorporating 1.6 mol.% of Fe_2O_3) at 90°C.

The presence of Fe in the glass also seems to delay the formation of a passivating gel during leaching in the $FeCl_2$ solution, but the mechanism appears to be different. During the (SBNFe; $FeCl_2$) experiment, Na and B are released congruently (Figure 8b), in agreement with literature data reporting that extensive leaching of alkalis is expected at the pH of the experiment [55]. The Fe cations resulting from the alteration of SBNFe (assumed to be in the +III oxidation state in the glass [18-20]) nevertheless appear to be retained in the gel, since leaching of SBN and SBNFe in the $FeCl_2$ solution leads to very different alteration kinetics

(Figure 8b). In the absence of charge compensating, *e.g.* by Na^+, Fe^{3+} incorporated into the gel structure cannot be in tetrahedral coordination. A change of Fe^{3+} from 4- to 6-coordination is then expected, as observed by Pèlegrin *et al.* [20] for the leaching of a more complex borosilicate glass. These authors conclude to the formation of hydrous Fe-oxyhydroxides (HFO) which are not linked to the silicate framework and do not have a passive role. The same type of mechanism could operate in the present study during the (SBNFe; $FeCl_2$) experiment. However, whatever the mechanism of Fe^{3+} incorporation into the gel, the resulting layer is not very passivating, as evident from the diffusion of Fe cations from the $FeCl_2$ supernatant through the gel formed on the SBNFe surface (Figures 5a and 5b).

3.4. Effect of Fe cations from the leaching supernatant

Numerous studies have shown that Fe presence in the medium where glass leaching takes place leads to the precipitation of Fe-silicates [14-17, 36, 47, 49], which appears to be the driving force sustaining glass alteration over time [14-16, 47]. Three mechanisms are generally invoked to explain this effect [16]:

(i) the overall uptake of Si present in the solution by precipitation of Fe-silicates, sometimes described as playing the role of a “silicon pump” [14-15, 17];
(ii) the penetration of Fe cations from the supernatant within the porous gel which leads to local consumption of Si by precipitation of Fe-silicates inside the gel porosity [14-17, 49];
(iii) the decrease in pH resulting from the precipitation of Fe-silicates.

In all the long-term experiments carried out in this study, a pseudo-steady-state [Si] is ultimately reached, which is close to the solubility of amorphous silica at the pH of each experiment (Figure 8c). This result appears to be consistent with the enrichment in Si (compared to the pristine glasses) of gel layers formed during long-term experiments (*cf.* subsection 3.2.1). In the case of experiments in the $FeCl_2$ solution, [Si] stabilizes after only three days of reaction at a value close to the solubility of amorphous silica at the pH of both experiments (Figure 8c). This suggests that the pseudo-steady-state [Si] observed during the leaching of SBN and SBNFe in the $FeCl_2$ solution should reach the same value regardless of precipitation of Fe-silicates; as long as glass alteration occurs at the same pH and leads to the formation of a similar gel.

Depth elemental profiles reported in Figure 5 have shown that the ingress of Fe cations from the leaching supernatant into the gel is not systematic and depends on the gel passivating properties. Even in the presence of dissolved Fe, a strongly passivating gel can form and prevent the ingress of Fe cations (mainly at the +II oxidation state), as demonstrated by the results of (SBN; $FeCl_2$) experiment (*cf.* subsection 3.2). On the other hand, the ingress of Fe cations from the supernatant into the gel layer was conspicuous for the (SBNFe; $FeCl_2$) experiment (Figures 5a and 5b). One can therefore wonder whether this ingress caused an increase in glass alteration, since it has been shown from experiments carried out in initially pure water that the presence of Fe in the glass composition is sufficient to delay the formation of a passivating layer (Figure 8a). In order to get a first answer, the overall increase in glass alteration related to the presence of Fe in the glass was estimated from the ratio of the altered glass fractions at the end of experiments in initially pure water ($I_{AG}^{H_2O}$) or in the $FeCl_2$ solution ($I_{AG}^{FeCl_2}$). The comparison of $I_{AG}^{H_2O}$ and $I_{AG}^{FeCl_2}$ values (Table 4) seems to show

that the increase in glass alteration due to combined effect of Fe present in the glass and diffusing from the supernatant is hardly greater than that due to the mere presence of Fe in the glass. This result suggests that the incorporation of Fe cations from the supernatant into the gel has little effect on the alteration of SBNFe in the $FeCl_2$ solution, at least with respect to the time scale investigated here.

In the case of our study, it is therefore the decrease in pH due to precipitation of Fe-silicates which seems to have the greatest impact on the alteration of SBN and SBNFe in $FeCl_2$ solution. This last conclusion is consistent with the work of Gin & Mestre [56] who studied the effect of pH on the leaching of SON68 glass during long-term experiments (about 600 days at 90 °C, S/V = 5000 m^{-1}). These authors showed that a decrease in the pH of the experiment from 9.5 to 7 leads to a sharp increase in glass alteration extent at the end of experiments. Over the same pH range, it was also shown that a decrease in the pH of the experiment delays the decrease in the glass alteration rate over time [56-57]. The last two findings are consistent with the differences in alteration kinetics of SBN and SBNFe between the experiments in initially pure water (average pH between 9.2 and 9.4) and those in the $FeCl_2$ solution (average pH between 6.1 and 6.3).

The results collected in this study convey a better understanding of the relative importance of the various processes by which precipitation of Fe-silicates can sustain glass alteration. Among the three mechanisms commonly invoked [16], it seems that the decrease in pH linked to the precipitation of Fe-silicates is preponderant, at least in the case of the alteration of SBN and SBNFe in $FeCl_2$ solution. The broad relevance of our conclusions must however be carefully assessed. Specifically, the effect of Fe migration from the leaching supernatant within the gel should be further scrutinized. A series of glass alteration experiments at the same pH and possibly the same [Si] values in leaching solutions containing or not Fe cations could improve our understanding of these processes. For this goal, a minimum [Fe] should always be maintained in order to avoid full uptake of Fe cations from the supernatant since this would cause significant pH variations (*cf.* subsection 3.2.2) which in turn may impact glass alteration [56-57]. It could also be interesting to work with a more complex glass, such as ISG, to be more representative of both the gel passivating properties and the nature of Fe-silicates formed during leaching of real nuclear glasses. This could be a first step toward linking studies on simple systems (as is the case here) and on much more complex systems, which have been more extensively studied. The later involve interactions between (i) glass, (ii) clay-based groundwater and (iii) corrosion products of Fe [14, 47-49], but also possibly (iv) metallic iron [14-15, 17, 36] sometimes coupled with the presence of (v) clay [17, 36].

4. Conclusion

This study brings new understandings on the effect of Fe on glass alteration, whether Fe is initially present in the glass composition or brought by the leaching supernatant.

The incorporation of Fe^{3+} cations in the glass composition has the same effect on glass alteration than that of Al^{3+}: the glass network is strengthened against hydrolysis reactions but restructuring of the gel into a passivating barrier is more difficult. This delay in passivation explain why the addition of Fe in the glass (at least for a content comparable to that studied here) ultimately leads to higher alteration extent. It can however be noted that even if the incorporation of Fe^{3+} cations within the gel systematically leads to a delay in passivation, the

cristallochemical environment of incorporated Fe^{3+} depends on the pH of the leaching solution. A change of Fe^{3+} from fourfold (*i.e.* charge compensated by Na^{+} ions) to sixfold coordination is thus expected when the pH decreases (from approximatively 9 to 6 in the present case), paralleling the greater leaching of alkalis.

In both experiments where Fe cations are provided by the leaching medium ($FeCl_2$ solution), the precipitation of Fe-silicates has been systematically observed. It is generally reported in the literature that this precipitation sustains glass alteration rates over a long period of time. This was not observed in our case for Fe-free glass leaching in $FeCl_2$ solution. During this experiment, the formation of a strongly passivating gel layer was demonstrated while a significant precipitation of Fe-silicates is also observed. The result of the leaching experiment carried out on the Fe-containing glass in $FeCl_2$ solution is more in accordance with literature data.

Several mechanisms have been proposed in previous studies to explain the detrimental effect of Fe-silicates precipitation on glass alteration. Among these, it seems that the decrease in pH resulting from the precipitation of Fe-silicates is the main cause of the increase in glass alteration observed in the present case.

Finally, it should be noted that these findings were obtained from a simple system. Their relevance needs to be carefully confirmed by additional studies before transposition to more complex systems, approaching the case of nuclear glass disposal in geological repository conditions.

Acknowledgements

The authors would like to thank EDF for its financial support. The authors would also like to thank Géraldine Parisot from the laboratory of long-term behavior of confinement matrix (CEA Marcoule, France), Michel Tabarant from the Laboratory for the Engineering of Surfaces and Lasers (CEA Saclay, France) and Laurent Dupuy from Biophy Research laboratory (Fuveau, France) for ICP-OES, GD-OES and ToF-SIMS analyses respectively.

References

[1] Dossier 2005 – Andra research on the geological disposal of high-level long-lived radioactive waste – Results and perspectives, Report Series, ANDRA, Châtenay-Malabry, 2005.

[2] P. Frugier, S. Gin, Y. Minet, T. Chave, B. Bonin, N. Godon, J. E. Lartigue, P. Jollivet, A. Ayral, L. De Windt, G. Santarini, SON68 nuclear glass dissolution kinetics: Current state of knowledge and basis of the new GRAAL model, J. Nucl. Mater. 380 (2008) 8-21.

[3] C. Poinssot, S. Gin, Long-term Behavior Science: The cornerstone approach for reliably assessing the long-term performance of nuclear waste, J. Nucl. Mater. 420 (2012) 182-192.

[4] G. Geneste, F. Bouyer, S. Gin, Hydrogen-sodium interdiffusion in borosilicate glasses investigated from first principles, J. Non-Cryst. Solids 352 (2006) 3147-3152.

[5] B. Grambow, H. U. Zwicky, G. Bart, I. K. Bjoerner, L. O. Werme, Modeling of the effect of iron corrosion products on nuclear waste glass performance, MRS Proc. 84 (1987) 471-481.

[6] C. Cailleteau, F. Angeli, F. Devreux, S. Gin, J. Jestin, P. Jollivet, O. Spalla, Insight into silicate-glass corrosion mechanisms, Nat. Mater. 7 (2008) 978-983.

[7] S. Gin, P. Jollivet, M. Fournier, F. Angeli, P. Frugier, T. Charpentier, Origin and consequences of silicate glass passivation by surface layers, Nat. Commun. 6 (2015).

[8] G. Bart, H. U. Zwicky, E. T. Aerne, T. Graber, D. Z'berg, M. Tokiwai, Borosilicate glass corrosion in the presence of steel corrosion products, MRS Proc. 84 (1987) 459-470.

[9] S. S. Kim, J. G. Lee, I. K. Choi, G. H. Lee, K. S. Chun, Effects of metals, metal oxides and metal hydroxide on the leaching of simulated nuclear waste glass, Radiochim. Acta 79 (1997) 199-205.

[10] Y. Inagaki, A. Ogata, H. Furuya, K. Idemitsu, T. Banba, T. Maeda, Effects of redox condition on waste glass corrosion in the presence of magnetite, MRS Proc. 412 (1995) 257-264.

[11] M.L. Schlegel, C. Bataillon, K. Benhamida, C. Blanc, D. Menut, J. L. Lacour, Metal corrosion and argillite transformation at the water-saturated, high-temperature iron-clay interface: A microscopic-scale study, Appl. Geochem. 23 (2008) 2619-2633.

[12] M. L. Schlegel, C. Bataillon, C. Blanc, D. Prêt, E. Foy, Anodic Activation of Iron Corrosion in Clay Media under Water-Saturated Conditions at 90 °C: Characterization of the Corrosion Interface, Environ. Sci. Technol. 44 (2010) 1503-1508.

[13] M. L. Schlegel, C. Bataillon, F. Brucker, C. Blanc, D. Pret, E. Foy, M. Chorro, Corrosion of metal iron in contact with anoxic clay at 90 degrees C: Characterization of the corrosion products after two years of interaction, Appl. Geochem. 51 (2014) 1-14.

[14] A. Michelin, E. Burger, E. Leroy, E. Foy, D. Neff, K. Benzerara, P. Dillmann, S. Gin, Effect of iron metal and siderite on the durability of simulated archeological glassy material, Corros. Sci. 76 (2013) 403-414.

[15] A. Michelin, E. Burger, D. Rebiscoul, D. Neff, F. Bruguier, E. Drouet, P. Dillmann, S. Gin, Silicate Glass Alteration Enhanced by Iron: Origin and Long-Term Implications, Environ. Sci. Technol. 47 (2013) 750-756.

[16] H. Aréna, N. Godon, D. Rébiscoul, P. Frugier, R. Podor, E. Garcès, M. Cabie, J. P. Mestre, Impact of iron and magnesium on glass alteration: Characterization of the secondary phases and determination of their solubility constants, Appl. Geochem. 82 (2017) 119-133.

[17] E. Burger, D. Rebiscoul, F. Bruguier, M. Jublot, J. E. Lartigue, S. Gin, Impact of iron on nuclear glass alteration in geological repository conditions: A multiscale approach, Appl. Geochem. 31 (2013) 159-170.

[18] N. Binsted, G. N. Greaves, C. M. B. Henderson, Fe K-edge X-ray absorption spectroscopy of silicate minerals and glasses, J. Phys. Colloques 47 (1986) C8-837-C8-840.

[19] K. E. Fox, T. Furukawa, W. B. White, Transition-Metal Ions in Silicate Melts. 2. Iron in Sodium-Silicate Glasses, Phys. Chem. Glasses 23 (1982) 169-178.

[20] E. Pèlegrin, G. Calas, P. Ildefonse, P. Jollivet, L. Galoisy, Structural evolution of glass surface during alteration: Application to nuclear waste glasses, J. Non-Cryst. Solids 356 (2010) 2497-2508.

[21] N. J. Cassingham, P. A. Bingham, R. J. Hand, S. D. Forder, Property modification of a high level nuclear waste borosilicate glass through the addition of Fe_2O_3, Glass Technol.: Eur. J. Glass Sci. Technol. A 49 (2008) 21-26.

[22] S. Gin, P. Frugier, P. Jollivet, F. Bruguier, E. Curti, New Insight into the Residual Rate of Borosilicate Glasses: Effect of S/V and Glass Composition, Int. J. Appl. Glass Sci. 4 (2013) 371-382.

[23] J. H. De Boer, The BET-Method, in: D. H. Everett, R. H. Ottewill (Eds.), Surface Area Determination, Butterworth & Co. Ltd., London, 1970, pp. 7-24.

[24] G. H. Jeffery, J. Bassett, J. Mendham, R. C. Denney, Vogel's textbook of quantitative chemical analysis, fifth ed., John Wiley & Sons, New York, 1989.

[25] S. Gin, X. Beaudoux, F. Angeli, C. Jegou, N. Godon, Effect of composition on the short-term and long-term dissolution rates of ten borosilicate glasses of increasing complexity from 3 to 30 oxides, J. Non-Cryst. Solids 358 (2012) 2559-2570.

[26] T. Chave, P. Frugier, S. Gin, A. Ayral, Glass–water interphase reactivity with calcium rich solutions, Geochim. Cosmochim. Acta 75 (2011) 4125-4139.

[27] S. Gin, P. Jollivet, G. Barba Rossa, M. Tribet, S. Mougnaud, M. Collin, M. Fournier, E. Cadel, M. Cabie, L. Dupuy, Atom-Probe Tomography, TEM and ToF-SIMS study of borosilicate glass alteration rim: A multiscale approach to investigating rate-limiting mechanisms, Geochim. Cosmochim. Acta 202 (2017) 57-76.

[28] S. Gin, P. Jollivet, M. Fournier, C. Berthon, Z. Wang, A. Mitroshkov, Z. Zhu, J.V. Ryan, The fate of silicon during glass corrosion under alkaline conditions: A mechanistic and kinetic study with the International Simple Glass, Geochim. Cosmochim. Acta 151 (2015) 68-85.

[29] J. Pons-Corbeau, Study of emission and sputtering yields in some alloys and oxide by glow discharge optical spectrometry: Quantification of analysis, Surf. Interface Anal. 7 (1985) 169-176.

[30] F. Jambon, L. Marchetti, F. Jomard, J. Chêne, Mechanism of hydrogen absorption during the exposure of alloy 600-like single-crystals to PWR primary simulated media, J. Nucl. Mater. 414 (2011) 386-392.

[31] M. Dumerval, S. Perrin, L. Marchetti, M. Tabarant, F. Jomard, Y. Wouters, Hydrogen absorption associated with the corrosion mechanism of 316L stainless steels in primary medium of Pressurized Water Reactor (PWR), Corros. Sci. 85 (2014) 251-257.

[32] J. Pons-Corbeau, J. P. Cazet, J. P. Moreau, R. Berneron, J. C. Charbonnier, Quantitative surface analysis by glow discharge optical spectrometry, Surf. Interface Anal. 9 (1986) 21-25.

[33] D. J. Backhouse, A. J. Fisher, J. J. Neeway, C. L. Corkhill, N. C. Hyatt, R. J. Hand, Corrosion of the International Simple Glass under acidic to hyperalkaline conditions, npj Mater. Degrad. 2 (2018) 29.

[34] C. Jégou, S. Gin, F. Larché, Alteration kinetics of a simplified nuclear glass in an aqueous medium: Effects of solution chemistry and of protective gel properties on diminishing the alteration rate, J. Nucl. Mater. 280 (2000) 216-229.

[35] I. S. Muller, S. Ribet, I. L. Pegg, S. Gin, P. Frugier, Characterization of Alteration Phases on HLW Glasses After 15 Years of PCT Leaching, in: C. C. Herman, S. Marra, D. Spearing, L. Vance, J. Vienna (Eds.), Environmental Issues and Waste Management Technologies in the Ceramic and Nuclear Industries XI, The American Ceramic Society, Westerville, 2006, pp. 189-199.

[36] G. de Combarieu, M. L. Schlegel, D. Neff, E. Foy, D. Vantelon, P. Barboux, S. Gin, Glass–iron–clay interactions in a radioactive waste geological disposal: An integrated laboratory-scale experiment, Appl. Geochem. 26 (2011) 65-79.

[37] N. Rajmohan, P. Frugier, S. Gin, Composition effects on synthetic glass alteration mechanisms: Part 1. Experiments, Chemical Geology 279 (2010) 106–119.

[38] B. Thien, N. Godon, F. Hubert, F. Angéli, S. Gin, A. Ayral, Structural identification of a trioctahedral smectite formed by the aqueous alteration of a nuclear glass, Appl. Clay Sci. 49 (2010) 135-141.

[39] K. Emmerich, Full Characterization of smectites, in: F. Bergaya and G. Lagaly (Eds.), Handbook of Clay Science – 2nd edition – Part B: Techniques and Applications, Elsevier, Amsterdam, 2013, pp. 381-404.

[40] M. Debure, L. De Windt, P. Frugier, S. Gin, P. Vieillard, Mineralogy and thermodynamic properties of magnesium phyllosilicates formed during the alteration of a simplified nuclear glass, J. Nucl. Mater. 475 (2016) 255-265.

[41] J. Wilson, G. Cressey, B. Cressey, J. Cuadros, K.V. Ragnarsdottir, D. Savage, M. Shibata, The effect of iron on montmorillonite stability. (II) Experimental investigation, Geochim. Cosmochim. Acta 70 (2006) 323-336.

[42] A. J. Spivack, M. R. Palmer, J. M. Edmond, The sedimentary cycle of the boron isotopes, Geochim. Cosmochim. Acta 51 (1987) 1939-1949.

[43] L. B. Williams, R. L. Hervig, J. R. Holloway, I. Hutcheon, Boron isotope geochemistry during diagenesis. Part I. Experimental determination of fractionation during illitization of smectite, Geochim. Cosmochim. Acta 65 (2001) 1769-1782.

[44] L. B. Williams, A. Turner, R. L. Hervig, Intracrystalline boron isotope partitioning in illite-smectite: Testing the geothermometer, Am. Mineral. 92 (2007) 1958-1965.

[45] B. A. Fleming, D. A. Crerar, Silicic acid ionization and calculation of silica solubility at elevated temperature and pH – Application to geothermal fluid processing and reinjection, Geothermics 11 (1982) 15-29.

[46] A. V. Bandura, S. N. Lvov, The Ionization Constant of Water over a Wide Range of Temperatures and Densities, J. Phys. Chem. Ref. Data 35 (2006) 15-30.

[47] P. Dillmann, S. Gin, D. Neff, L. Gentaz, D. Rebiscoul, Effect of natural and synthetic iron corrosion products on silicate glass alteration processes, Geochim. Cosmochim. Acta 172 (2016) 287-305.

[48] N. Godon, S. Gin, D. Rebiscoul, P. Frugier, SON68 glass alteration enhanced by magnetite, Procedia Earth Planet. Sci. 7 (2013) 300-303.

[49] D. Rebiscoul, V. Tormos, N. Godon, J. P. Mestre, M. Cabie, G. Amiard, E. Foy, P. Frugier, S. Gin, Reactive transport processes occurring during nuclear glass alteration in presence of magnetite, Appl. Geochem. 58 (2015) 26-37.

[50] M. Pijolat, M. Soustelle, Experimental tests to validate the rate-limiting step assumption used in the kinetic analysis of solid-state reactions, Thermochim. Acta 478 (2008) 34-40.

[51] W. G. Ramsey, T. D. Taylor, C. M. Jantzen, Predictive modeling of leachate pH for simulated high-level waste glass, in: G. G. Wicks, D. F. Bickford (Eds.), Nuclear Waste Management IV – Ceramic Transactions Vol. 23, The American Ceramic Society, Westerville, 1991, pp. 105-114.

[52] A. Ledieu, F. Devreux, P. Barboux, The role of aluminium in the durability of alumino-borosilicate glasses, Phys. Chem. Glasses 46 (2005) 12-20.

[53] F. Angeli, T. Charpentier, S. Gin, J. C. Petit, ^{17}O 3Q-MAS NMR characterization of a sodium aluminoborosilicate glass and its alteration gel, Chem. Phys. Lett. 341 (2001) 23-28.

[54] S. Kerisit, J. V. Ryan, E. M. Pierce, Monte Carlo simulations of the corrosion of aluminoborosilicate glasses, J. Non-Cryst. Solids 378 (2013) 273-281.

[55] B. C. Bunker, Molecular mechanisms for corrosion of silica and silicate glasses, J. Non-Cryst. Solids 179 (1994) 300-308.

[56] S. Gin, J.-P. Mestre, SON 68 nuclear glass alteration kinetics between pH 7 and pH 11.5, J. Nucl. Mater. 295 (2001) 83-96.

[57] D. Strachan, Glass dissolution as a function of pH and its implications for understanding mechanisms and future experiments, Geochim. Cosmochim. Acta 219 (2017) 111-123.